Effect of the chain on thermal conductivity and thermal boundary conductance of long chain n-alkanes using molecular dynamics and transient plane source techniques

by

Rouzbeh Rastgarkafshgarkolaei

A thesis submitted to the Graduate Faculty of
Auburn University
in partial fulfillment of the
requirements for the Degree of
Master of Science

Auburn, Alabama
August 2, 2014

Keywords: Molecular Dynamics, N-alkanes, Nanoscale Thermal Transport, Phase Change Materials, Thermal Boundary Conductance, Thermal Conductivity

Approved by

Jay M. Khodadadi, Chair, Alumni Professor, Department of Mechanical Engineering
Daniel Harris, Associate Professor, Department of Mechanical Engineering
Minseo Park, Professor, Department of Physics

Abstract

The effect of the length of the long chain n-alkane molecules on the nanoscale thermal transport within various phases of n-alkanes is investigated. The thermal conductivity of the n-alkanes is determined using both molecular dynamics (MD) simulations and transient experiments. Molecular dynamics simulations have also been utilized to investigate the thermal boundary conductance between the layers of perfect crystal n-alkanes.

The thermal conductivity of four (4) n-alkanes including $C_{20}H_{42}$, $C_{24}H_{50}$, $C_{26}H_{54}$ and $C_{30}H_{62}$ was determined in the liquid, solid and perfect crystal phases using the non-equilibrium molecular dynamics (NEMD) method. In the direct NEMD approach, heat flux is imposed over the sample and the associated temperature profile is obtained after the system reaches the steady state. Thermal conductivity values for liquid n-alkanes increase as the number of carbon atoms within the chain is raised which is consistent with the available experimental trend for liquid n-alkanes. Liquid systems were then cooled down to obtain the solid phase n-alkane structures whereby randomly oriented molecules in the liquid mode reorganize into crystalline nano-domain structures. The degree of structural organization is quantified through using the alignment factor. The more organized solid structures of the solid phase n-alkanes accommodate higher thermal conductivity values compared to the liquid systems which can be observed in thermal conductivity results for the solid structures. However, for the case of the solid n-alkanes, there was no distinct relation between the thermal conductivity and the length of the n-alkane

molecule. The thermal conductivity of $C_{24}H_{50}$ was higher than the corresponding value for $C_{20}H_{42}$. As the number of the carbon atoms within the molecules increase from n=24 to n=26, the thermal conductivity remained almost unchanged. The thermal conductivity of $C_{30}H_{62}$ was the highest among the n-alkanes investigated. In general, there is an increase in the thermal conductivity of solid n-alkanes as the length of the n-alkane molecules increases. The possible effect of anisotropy of the thermal conductivity tensor due to the structural organization of the solid phase was investigated and was shown to be negligible. Perfect crystal n-alkanes serve as ideal models of structural organization with perfect alignment in a hexagonal lattice. For this model, all the n-alkane molecules are aligned in the direction of molecular axis which gives the highest possible thermal conductivity of the n-alkanes. Perfect crystal n-alkanes exhibit a zigzag trend for the thermal conductivity values as the number of the carbon atoms within n-alkane molecules increases.

Experiments were carried out to measure the thermal conductivity of three (3) solid n-alkanes (n = 20, 24 and 26) using the transient plane source (TPS) method. The experimental thermal conductivity values of $C_{20}H_{42}$ agreed well with previous measured data of other researchers. It was shown that the thermal conductivity values of $C_{20}H_{42}$ and $C_{24}H_{50}$ are very close to each other, whereas the thermal conductivity decreased for $C_{26}H_{54}$.

MD simulations have also been utilized to investigate the thermal interfacial conductance between the layers of perfect crystal n-alkanes. Both equilibrium and non-equilibrium molecular dynamics (EMD and NEMD, respectively) methods were used to determine the thermal boundary conductance. The EMD method uses the Green-Kubo relation for determining the thermal boundary conductance through relating the power fluctuations across the interfaces to the thermal boundary resistance. In the NEMD method, the temperature drop/rise across each

interface was related to the thermal boundary conductance between the neighboring layers. Results from both methods exhibit no dependency of the thermal boundary conductance on the length of the n-alkane molecules. However, the thermal boundary conductance values obtained from the EMD simulations are less than the values from the NEMD simulations where this difference reaches a factor of nearly five (5) in most cases.

Acknowledgments

I am grateful to my lovely family for their kind support during the years of my education and specially my two years of master's degree in Auburn University where I was away from my family. My family played the most important role in putting me on the path toward this goal. My lovely mother always supported me unconditionally and provided me with her mental support. My father, whose major was economics, got me interested to math and science and his support helped me through in this way. My brother, who is a mechanical engineer, certainly influenced me to pursue mechanical engineering. My lovely sisters consistently improved my belief of achievement. I am extremely appreciative to all of them.

I am grateful to my advisor, Dr. Jay M. Khodadadi, for his great support and advice, who sparked my interest in nanoscale thermal transport when I just came to Auburn. He was always advising me to realign myself in the right path for achieving my goals. He always included me in great scientific experiences that I am grateful for all of them. I am so proud that I have his trust in my research. More importantly, he opened my eyes on life with his great talks in our spare times after each meeting. I learned a lot from him and I never forget his lessons.

I would like to thank Mr. Hasan Babaei, my great colleague in Dr. Khodadadi group. He was the one who helped me through my research and I learned a lot from our great talks on new topics in this area. Whenever I had got any problem with the simulations, he was there to listen to me kindly and motivate me to solve the problem. I want to thank Mr. Nabil who helped me to

begin working with my experiments. I would like to thank to my other colleagues Dr. Moeini Sedeh and Dr. El Hasadi whom I learned a lot by sharing my time with them talking about different aspects of our research.

I am also grateful to Dr. Minseo Park of the Department of Physics at Auburn University, who I learned from his lectures in his course, "Solid State Physics". I am proud that he is serving as the committee member for my thesis.

I would also like to thank Dr. Daniel Harris of the Department of Mechanical Engineering, for serving as the committee member and for his informative graduate course that I have taken during my first semester in Auburn University.

I acknowledge the Department of Mechanical Engineering and the Samuel Ginn College of Engineering at Auburn University for their support of my graduate fellowship through providing a teaching assistantship and financial support, respectively.

This thesis is based upon the work partially funded by the United States Department of Energy under the Award Number DE-SC0002470. This report was prepared as an account of work sponsored by an agency of the United States Government. Neither the United States Government nor any agency thereof, nor any of their employees, makes any warranty, express or implied, or assumes any legal liability or responsibility for the accuracy, completeness, or usefulness of any information, apparatus, product, or process disclosed, or represents that its use would not infringe privately owned rights. References herein to any specific commercial product, process, or service-water by trade name, trademark, manufacturer, or otherwise does not necessarily constitute or imply its endorsement, recommendation, or favoring by the United

States Government or any agency thereof. The views and opinions of authors expressed herein do not necessarily state or reflect those of the United States Government or any agency thereof.

Few data in this material are reproduced with permission of Elsevier and Springer.

Table of Contents

List of Tables

List of Figures

List of Abbreviations

AMM	Acoustic Mismatch Model
AUA	Anisotropic United Atom
DMM	Diffusive Mismatch Model
EMD	Equilibrium Molecular Dynamics
HCACF	Heat Current Auto-Correlation Function
LAMMPS	Large-scale Atomic/Molecular Massively Parallel Simulator
MD	Molecular Dynamics
N-alkane	Normal Alkane
NePCM	Nano Enhanced Phase Change Materials
NEMD	Non-Equilibrium Molecular Dynamics
NERD	Nath, Escobedo and de Pablo-Revised
OPLS	Optimized Potentials for Liquid Simulations
PACF	Power Auto-Correlation Function
PCM	Phase Change Materials
R Phase	Rotator Phase

SKS	Smit, Karaborni and Siepmann
TPS	Transient Plane Source
TraPPE	Transferable potentials for phase equilibria
UA	United Atom

List of Symbols

Nomenclature

A	Cross Section Area, m^2
C	Parameter Related to Phonon Properties, m^2K/W
E	Internal Energy, J
$F\ (i)$	Force acting on the particle i, N
G_k	Thermal Boundary Conductance, W/m^2K
$J_i(t)$	Heat Current, W
k	Thermal Conductivity, W/mK
k_B	Boltzmann Constant, m^2 kg/ s^2k
L	Length of the Simulation Box, m
$m\ (i)$	Mass of the Particle i, kg
$p\ (i)$	Momentum of the Particle i, N s
$P(t)$	Heat Power, W
q	Heat Flux, W/m^2

$r(i)$	Position of the Particle i , m
s	Orientation Factor
T	Temperature, K
t	Time Instant, s
U	System Potential Energy, J
V	Potential Energy, J
V	Volume of the Simulation Box, m^3
X, Y, Z	Distance, m

Greek Symbols

θ	Angle between the end-to-end vector a molecule and an axis
θ	Bond Angle
σ	Van Der Waals Radius (length scale), Å
ψ	Torsional Angle
ϵ	Potential Well Depth, J

Subscripts

∞	Infinity, introduced in equation (2.7)
B	Boltzmann
eq	Equilibrium
i	Index for a Particle, introduced in equation (2.3)
i	*x, y* or *z*
k	Kapitza, introduced in equation (2.8)
LJ	Lennard-Jones
r	Radius
θ	Angle

1. Chapter One: Introduction

1.1 Background and Motivation

The rapid growth of technology over the last two centuries has led to a very high rate of increase of demand for energy. Even though fossil fuels are cheap and generally easy to access, the growing consumption of such fuels is of great concern due to environmental pollution issues. Therefore, scientists/engineers are greatly interested to replace the fossil fuels with environment-friendly renewable sources of energy, including solar, wind and wave energy. However, renewable sources of energy have a major drawback having to do with their unpredictable availability. Thus, energy storage has been identified as the critical bottleneck to the widespread adoption and utilization of the renewable energy sources. In particular, storing of thermal energy (also applicable to waste heat recovery) can be achieved through three distinct modes: 1- Sensible heat storage, 2- Latent heat storage and 3- Chemical energy storage. Sensible storage is the process of storing thermal energy through a temperature change in the material in one phase and utilizes a material's heat capacity which is known as the specific heat. Latent storage is the process of achieving thermal energy storage upon melting and releasing the absorbed energy during freezing of a material at a nearly constant temperature. Instantaneous temperature of a typical phase change material (PCM) during heating and cooling near its fusion (melting) temperature are shown in Figure 1-1 that depicts both sensible and latent modes of thermal energy storage.

A variety of PCM are used as the media for latent heat storage. Water, aqueous salt solutions, sugar alcohols, paraffins, etc. are typical phase change materials possessing a wide range of melting temperatures and heat of fusion (Figure 1-2). In choosing an appropriate PCM, one needs to consider many important factors. A number of such factors are listed in Table 1-1. The PCM must have a melting point in the range of the system's working temperature. Many groups

of materials classified as PCM (e.g. fluorides, nitrates, etc.) cover a wide range of melting temperatures (Figure 1-2). The target PCM should also have high enough energy storage density, be chemically stable and possess a high value of thermal conductivity. Properties of different groups of PCM (organic and inorganic) are summarized in Table 1-2. Among these properties, thermal conductivity is one of the most critical properties that affects the charge/discharge of thermal energy during the cyclic freeze/thaw cycles. Even though a variety of PCM are available for specific applications, their thermal conductivity is generally low, thus limiting the performance of the thermal storage system that will utilize the PCM. Thermal conductivity values for some widely-used PCM are reported in Table 1-3 that helps the reader to compare the relative thermal conductivity values of such materials.

Normal alkanes, also called linear alkanes (C_nH_{2n+2}) and paraffins, are the most commonly-used materials as PCM. N-alkanes exhibit small or no degree of supercooling in their melting and solidifying cycles and they have moderate thermal energy storage density. Interestingly, n-alkanes with an odd number of carbon atoms (n-odd alkanes) behave differently when compared to n-even alkanes (Ryckaert and Klein, 1986, and Yarbrough and Kuan, 1981). Research efforts have been devoted to this interesting phenomenon (polymorphism) to uncover the reasons for such behavior. Polymorphism of n-alkanes can be described in the way that molecules with odd and even numbers of carbon atoms exhibit different crystal structures at low temperatures in their solid phases. In effect, different trends for the thermodynamic properties of odd and even n-alkanes, such as the equilibrium melting point (Boese et al., 1999) and also thermal conductivity of n-alkanes (Yarbrough and Kuan, 1981)) are observed. Moreover, n-even alkanes exhibit a degree of supercooling of more than 3 °C which are not observed in n-odd alkanes phase diagrams. Between the low-temperature highly-ordered solid structures and the liquid phase,

there exist a series of weakly-ordered crystalline phases near the melting point which are called the “rotator (R) phases”. To date, five (5) different R-phases for n-alkanes have been identified. In the previous studies, different thermodynamic behaviors of n-alkanes were related to the existence of different R-phases right before melting. For instance, it is believed that the presence of the R-phase at the surface near the crystallization point can serve as an ideal nucleation site for crystallization which can be the reason behind the lack of supercooling in n-odd alkanes. Researchers have long been interested to understand how thermal conductivity changes with different factors for n-alkanes. Rastorguev et al. (1974) stated that their experimental findings exhibited a linear rise in thermal conductivity in the liquid phase as the number of carbon atoms in the chain of n-alkanes is increased. Compared to other types of PCM, n-alkanes exhibit low thermal conductivity. Great effort has been applied to improve the thermal conductivity of paraffin-based thermal energy storage systems (Fan and Khodadadi, 2011). For instance, introduction of high thermal conductivity nanoparticles and high aspect-ratio nano-scale highly-conductive materials into PCM in general and n-alkanes in particular, has gained great interest in recent years (Khodadadi et al., 2013).

Conductive (diffusive) heat transfer within materials is governed by the Fourier’s law where heat is being carried by the phonons. Phonon is the elementary vibration of atoms and molecules within the lattice structure with a specific frequency. As the size of system shrinks, phonon scattering within the interfaces can change which affects the transport of heat. Therefore, phonon transport must be studied in detail to get more insight into the dominant transport mechanisms within the devices with nanoscale size.

Molecular dynamics (MD) simulations is a strong candidate to study the nanoscale transport phenomena within a variety of materials. Molecular dynamics simulations have been widely

used in recent years to study the interfacial conductance between the layers and identify the dominant transport mechanisms related to thermal conductivity measurements. Utilizing MD simulations, one can understand and analyze the motion and dynamics of atoms and molecules within the PCM.

1.2 Objectives and outline of the thesis

The objective of this thesis is to investigate the effect of the length of the longer chain n-alkane molecules on the thermal transport within these molecules. The studied n-alkanes are the ones that have the great potential of being applied as PCM in thermal energy storage systems. To address this effect, MD simulations have been carried out to determine the thermal conductivity of bulk n-alkanes in both liquid phase and solid structures. Moreover, n-alkanes with ideal perfect crystal structures have been tested to estimate the maximum possible thermal conductivity of the n-alkanes. Thermal boundary conductance between the layers of perfect crystal n-alkanes is investigated as well.

Additionally, experiments have been conducted to measure the thermal conductivity of solid n-alkanes experimentally. In this regard, a state-of-the-art transient plane source (TPS) apparatus is utilized to measure the thermal conductivity of the PCM.

This thesis is organized as follows:

Chapter 2 discusses the details of MD simulations and methodologies. The methods of numerical integration of the equation of motion are explained. The interatomic potentials (force fields) that are used in this work are defined. Then, the direct method of determining the thermal conductivity and thermal boundary conductance (non-equilibrium molecular dynamics) is explained in detail. A second MD-based method (Green-Kubo method) is also discussed.

Chapter 3 is devoted to the thermal conductivity of the n-alkanes. Firstly, n-alkanes are introduced followed by a study of the thermal conductivity of the n-alkanes using direct method MD simulations. At last, an experimental approach of preparing n-alkane solid samples and measuring their thermal conductivity using the TPS method is discussed.

In chapter 4, the thermal boundary conductance between the layers of perfect crystal n-alkanes utilizing MD simulations using two methods (direct method and Green-Kubo method) is discussed. The results from the direct and Green-Kubo methods are compared lastly.

Table 1-1: Important properties of PCM

Heat of fusion	High
Thermal conductivity	High
Density	High
Specific heat	High
Volume change	Low
Vapor pressure	Low
Stability	Chemical stability in response to exposures
Cycling stability	$\geq$ 1000
Supercooling	Small
Compatibility	With container material
Price	Low
Recyclability	Desired

Table 1-2: Critical properties of different PCM (data from Mehling and Cabeza, 2008)

PCM	Melting temperature	Storage density	Phase separation	Super-cooling degree	Volume change	Corrosion	Chemical stability
Eutectic water-salt solutions	< 0 °C	good	Possible	High	High (5-10%)	Corrosive to metals	Stable
Salt hydrates	5-130 °C	high	Possible	high	High (up to 10%)	Corrosive to metals	Very stable
Paraffins	0-200 °C	good	-	Little or no supercooling	High (10%)	Not corrosive to metals	Stable but not stable at higher temperatures
Fatty acids	0-200 °C	good	-	Little or no supercooling	-	Corrosive to metals	Stable but not stable at higher temperatures
Sugar alcohols	90-200 °C	high	-	Some	-	Soft	Not stable at higher temperatures

Table 1-3: Thermal conductivity values of some common PCM (data from Mehling and Cabeza, 2008)

Material	**Thermal conductivity (W/ m K)**
Water (liquid, 20 °C)	**0.6**
Water (solid, 0 °C)	**2.2**
$CaCl_2.6H_20$ (liquid, 39 °C)	0.54
$CaCl_2.6H_20$ (solid, 23 °C)	1.088
$LiNO_3$ (liquid)	0.58
$LiNO_3$ (solid)	1.37
n-Tetradecane (solid) $C_{14}H_{30}$	0.21
n-Octadecane (liquid, 40 °C) $C_{18}H_{38}$	**0.148**
n-Octadecane (solid, 25 °C) $C_{18}H_{38}$	**0.358**

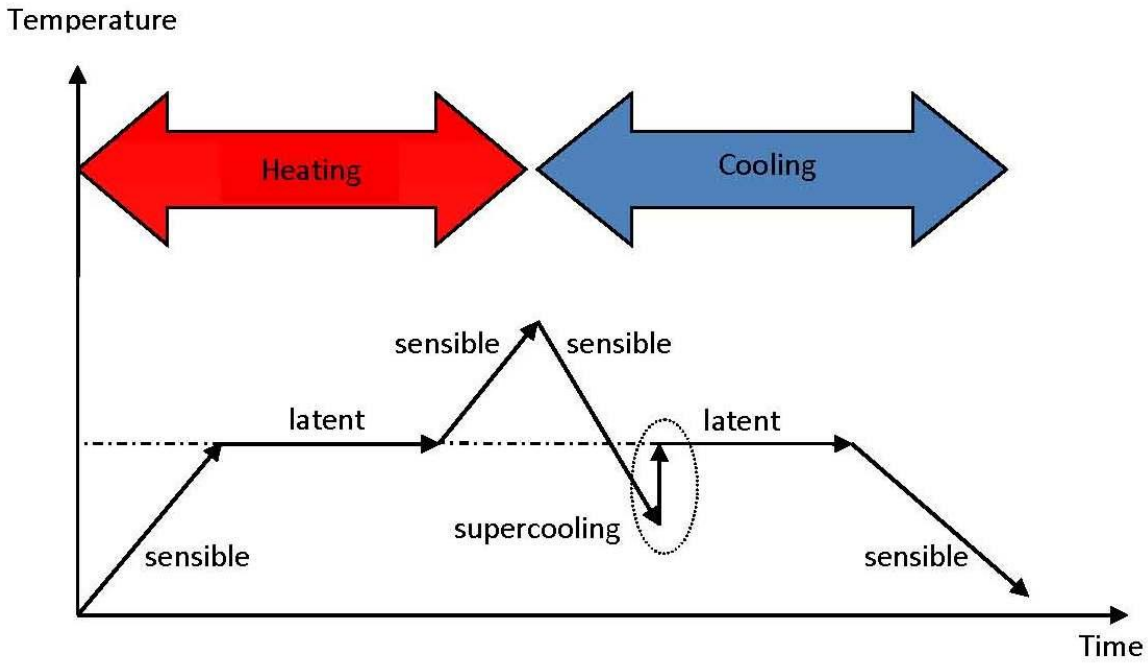

Figure 1-1: Schematic diagram of temperature change of PCM during melting and consequent solidification with possible supercooling during freezing (extracted and reworked from Mehling and Cabeza, 2008)

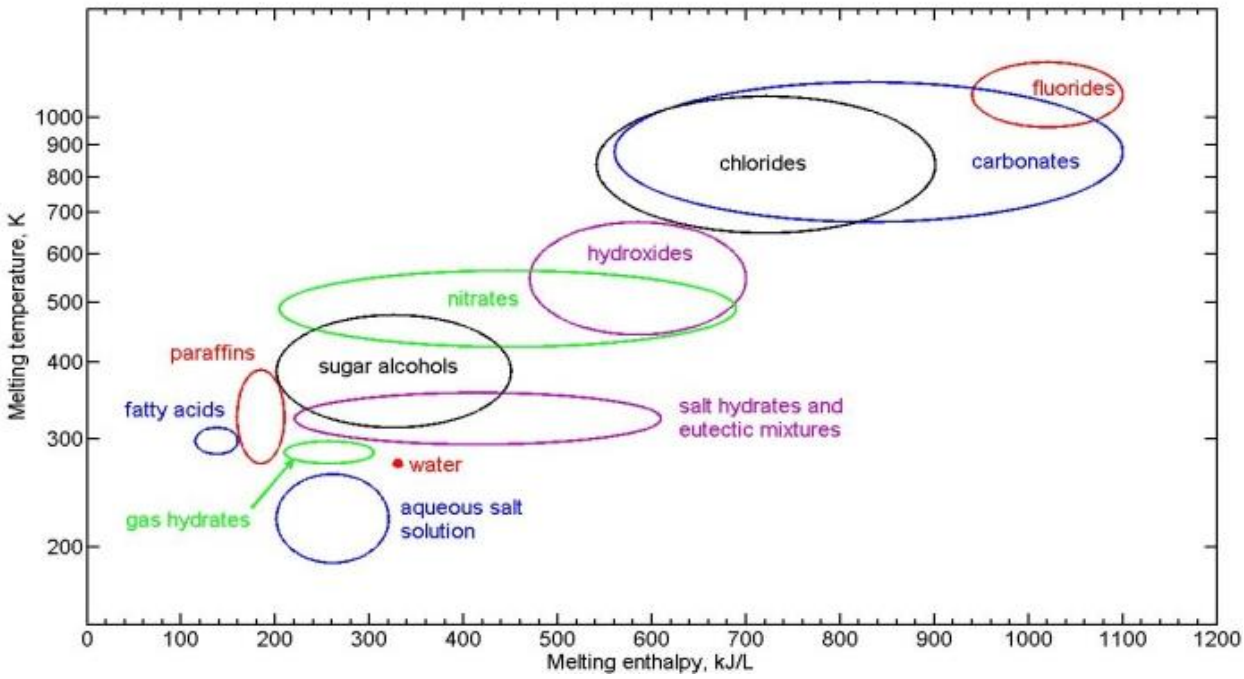

Figure 1-2: Groups of materials widely used as PCM with their associated range of melting temperature and latent storage potential (extracted from Fan, 2011)

2. Chapter Two: Molecular Dynamics Simulations

2.1 Overview:

Molecular dynamics (MD) simulations have been utilized to study the transport phenomena at the nanoscale. Moreover, MD simulations have been widely used to study the thermal transport within different phases of a variety of materials. In effect, MD simulation is considered to be a powerful tool that provides observation of a system with atomic-scale resolution. Despite the fact that MD simulations are simple in principle, there might be a dark side for these simulations that need to be considered crucial to all simulations and a very careful study is needed to verify the results (Frenkel, 2013).

In a MD simulation, the positions and momenta of the atoms/molecules are determined by integrating the governing Newton's equations of motion. The only input that is needed to perform a MD simulation is an appropriate function that specifies the atomic interactions which is called the atomic force field.

There are two notable restrictions for a MD simulation. Firstly, MD simulation neglects the motion of electrons, thus it is limited to materials for which thermal transport is mostly governed by the phonon transport. In this thesis, thermal transport within n-alkanes which are considered to be phonon-dominated heat transfer materials will be studied (Murashov and White, 2004). Secondly, because the motion of atoms/molecules is specified by the Newton's equations of motion, the atomic dynamics in MD simulation are classical. In addition, the MD-predicted properties in this thesis are evaluated at temperatures near or above the Debye temperature to minimize the quantum effects.

2.2 Integration of the Newton's equation of motion:

A variety of algorithms have been developed to numerically integrate the simultaneous Newton's equations of motion in an MD simulation involving a great number of atoms. These include the velocity Verlet, Verlet leapfrog and Gear predictor-corrector algorithms. These algorithms are employed to predict the motion of atoms at the time instant $t+\Delta t$ based on the position and momenta at a previous time instant t. Smaller values of the time step, Δt, will lead to a lower numerical error. In this thesis, the velocity Verlet algorithm is chosen over other algorithms because of its ease of implementation. The force acting on the particle i, i.e. $F(i)$, is the partial derivative of the total system potential energy, U, which reads as

$$F(i) = \frac{\partial U}{\partial r(i)}. \tag{2.1}$$

with $r(i)$ standing for the position vector for atom i. Knowing about the initial position and momentum of one particle, the Verlet algorithm can be utilized to predict the motion of the particle at the end of the time step using the Taylor series expansion of the expressions for the position and momentum of the particle, i.e.,

$$p\left(i, t + \frac{\Delta t}{2}\right) = p(i,t) + \frac{F(i,t)\Delta t}{2} \tag{2.2}$$

$$r\left(i, t + \frac{\Delta t}{2}\right) = r(i,t) + p\left(i, t + \frac{\Delta t}{2}\right)\Delta t/m_i \tag{2.3}$$

$$p\,(i, t + \Delta t) = p\left(i, t + \frac{\Delta t}{2}\right) + \frac{F(i,t+\Delta t)\Delta t}{2}. \tag{2.4}$$

In the relations above, m_i stands for the mass of atom i, whereas $r(i,t)$ and $p(i,t)$ are the position and momentum vectors of atom i, respectively. A schematic view of the system of atoms along with the pertinent interaction parameters is shown in Figure 2-1.

A very important factor in MD simulations is the value of the time step. This value should be small enough so that the total energy of the system under study, *E,* is conserved within the whole simulation. Landry (2009) used a general rule of choosing the suitable time step and that is to choose the time step such that $1/\Delta t$ is one to two orders of magnitude greater than the maximum vibrational frequency in the system. It has been shown in previous inelastic neutron scattering studies that molecular motions in n-alkanes on a time scale of 10^{-12} seconds are associated with phase change (Barnes, 1973). In this thesis, we study n-alkanes and the value of time step is chosen to be 0.5 fs (0.5×10^{-15} seconds).

2.3 Interatomic Potentials:

An MD simulation is in need of only one type of input and that is the interatomic potential which is also called the force-field. A force-field describes the potential energy of a system of molecules/atoms.

The Lennard-Jones potential (Lennard-Jones, 1924) which is referred to as the L-J potential, is a form of potential that describes the interaction between two neutral particles. In this model, the particles are modeled as spherical balls. The mathematical model for this potential in the most common way reads as

$$V_{LJ} = 4\epsilon \left[\left(\frac{\sigma}{r}\right)^{12} - \left(\frac{\sigma}{r}\right)^{6} \right], \tag{2.5}$$

where ϵ is the potential well depth (energy scale), σ is the van der Waals radius (length scale) and r is the distance of separation between two particles (Figure 2-1). A cut-off radius is used to make the calculation process in molecular modeling faster and that is to ignore the van der Waals interaction energy for pairs with the respective distance being greater than the cut-off radius. The cut-off radius is usually taken to be $2.5\sigma_{LJ}$.

In this thesis, we study the thermal transport within long chain n-alkanes. There are various force-fields for n-alkanes. The four (4) most suitable force-fields for molecular modeling of n-alkanes are the OPLS (Optimized Potentials for Liquid Simulations) credited to Jorgensen et al. (1984), TraPPE (Transferable potentials for phase equilibria) introduced by Martin and Siepmann (1998), SKS (Smit, Karaborni and Siepmann, 1995) and NERD (Nath, Escobedo and de Pablo-revised) credited to Nath et al. (1998). All of these force-fields utilize mathematical functions to describe the interaction between the particles considering pairwise interactions, bond stretching, bond bending and dihedral torsion of such molecules. The differences among these force-fields are due to the parameters of the respective mathematical functions.

The NERD is a united atom (UA) potential that considers CH_2- and CH_3- groups as interaction sites (Figure 2-1). The Anisotropic united atom (AUA) model which is also called the full atomic model is more realistic than the UA potential since this model considers the hydrogen atoms in the chains explicitly. However, it is mentioned in previous studies (Martin and Siepmann, 1998) that the AUA model is computationally very time-consuming and will introduce unnecessary complications through explicit representation of the hydrogen atoms.

Babaei (2013a) found that the NERD potential is the most appropriate force-field to investigate the thermal transport within the long chain n-alkanes. Table 2-1 summarizes the mathematical equations for the NERD force-field.

For the non-bonded intermolecular atoms or atoms belonging to the same molecules but at least four bounds away, the pair potential is that of the Lennard-Jones model with the parameters that are summarized in Table 2-2. The cut-off radius in this thesis was chosen to be 10 $\mathring{A}$.

2.4 MD Ensembles:

There are three mostly discussed equilibrium ensembles in statistical thermodynamics for any isolated system inside a specific volume. These ensembles correspond to classical thermodynamics in the macroscopic limit.

The NVE ensemble, also known as the microcanonical ensemble, describes a system with a fixed number of atoms, *N*, volume, *V*, and the total energy of the system, *E*.

The isothermal-isobaric ensemble (NPT), also known as the grand canonical ensemble, describes a system with fixed pressure and temperature. It is sometimes desired to set the pressure and temperature of the system in an MD simulation. The system can then be allowed to equilibrate under the NPT ensemble at the desirable values of pressure and temperature.

Under the conditions of the NVT ensemble, also known as the canonical ensemble, the temperature of the system is fixed without setting any value for pressure. In this ensemble, the volume of the system will be held fixed during the simulation.

2.5 NEMD Direct Method for Prediction of the Thermal Conductivity and Thermal Interfacial Conductance

The direct method is a nonequilibrium, steady state MD approach that can be used to determine the thermal conductivity of a structure or the thermal interfacial conductance between the layers of the molecules. In this method, a known heat flux is imposed along one direction that in turn gives rise to a temperature profile. The thermal conductivity can then be determined using the Fourier's law:

$$\bar{q} = -\bar{\bar{k}}\,\nabla T, \tag{2.6}$$

where $\bar{q}$ is the heat flux vector, $\bar{\bar{k}}$ is the thermal conductivity tensor and ∇T is the temperature gradient vector. A constant amount of kinetic energy is exchanged between a hot and a cold slab to generate the heat flux (Schelling et al., 2002). The value of the heat flux should be chosen in a way that the resulting temperature drop in the simulation box is greater than the statistical temperature fluctuations (Landry, 2009). Figure 2-2 exhibits a schematic view of the system with the adopted heat sink and sources. Periodic boundary conditions are imposed in all three spatial directions. It is also possible to utilize one sink and one source in the system that should lead to similar results we obtained using the arrangement shown in Figure 2-2.

One challenge in utilizing the NEMD direct method is to remove the size effect from the MD-predicted values for the thermal conductivity. The size effect is mainly due to Phonon dynamics within the simulation box and it has been mentioned that phonon scattering in the vicinity of sink/source is one cause for this effect. Schelling et al. (2002) stated that in an NEMD direct method simulation, the effect of the size of the simulation box should be studied. To remove the size effect, the thermal conductivity values for different sizes of the structure should be obtained. The inverse of thermal conductivity values will then be plotted vs. the inverse of the length of the simulation box. One can determine the thermal conductivity of the system with the length of infinity ($L \to \infty$) using an extrapolation from the resulting graph. The extrapolation procedure explained here is based on the assumption that the thermal conductivity of an isotropic system is a function of the length of sample and the phonon properties, or equivalently,

$$\frac{1}{k} = \frac{1}{k_\infty} + \frac{C}{L}, \tag{2.7}$$

where k_∞ is the macroscopic thermal conductivity and C is related to the phonon properties. Sellan et al. (2010) stated that increasing the simulation cell size simply to remove the cell size

effect has a limitation. They found that increasing the size might result in over-estimation of the thermal conductivity values. They proved that the systems with a minimum size of the largest mean free path of the effective phonon modes in thermal transport should be utilized to predict the macroscopic thermal conductivity.

The NEMD method is also utilized to determine the thermal interfacial conductance between the layers of perfect crystal n-alkanes. Temperature profile associated with the imposed heat flux was collected from the MD simulations. There is a temperature jump between each two neighboring layers of the perfect crystal n-alkane molecules. Thermal interfacial conductance can be calculated using the formula:

$$G_k = \frac{q}{\Delta T}, \tag{2.8}$$

where q is the value for the imposed heat flux and ΔT is the average of all the temperature differences between the neighboring layers.

2.6 Equilibrium Molecular Dynamics Green-Kubo Method

The Green-Kubo method relates the fluctuating dynamical variables of the systems in equilibrium to their transport properties (Kubo, 1957, and Vogelsang et al., 1987). The equilibrium molecular dynamics (EMD) Green-Kubo method has been widely used to determine the thermal conductivity of the material utilizing the relation below:

$$k_{ii} = \frac{V}{k_B T^2} \int_0^\infty < J_i(t) J_i(0) > dt, \quad i = x, y \text{ or } z \tag{2.9}$$

where the symbol < > denotes ensemble average, V is the volume of the simulation box, k_B is the Boltzmann constant, t is time and J is the heat current which is obtained from the simulations. By

integrating the heat current autocorrelation function (HCACF) over time, the *i*-th diagonal component of the thermal conductivity matrix is calculated at temperature *T*.

In this thesis, however, the Green-Kubo method has been used to predict the thermal interfacial conductance (G_k) between the layers of the perfect crystal n-alkanes. The Green-Kubo formula for calculating the thermal interfacial conductance is as follow:

$$G_k = \frac{1}{Ak_BT^2}\int_0^\infty < p(t)p(0) > dt, \tag{2.10}$$

where *A* is the cross sectional area of the solid interface and *p* is the fluctuating heat power across the interface which can be computed by $p(t) = dE(t)/dt$, with *E* standing for the instantaneous internal energy of the layer of molecules that is obtained from the simulations.

The structure was equilibrated under the NPT ensemble for 3,000,000 time steps. The total energy of the middle layer then was recorded every five (5) time steps for 2,000,000 time steps under the NVE ensemble for calculating the power and the auto-correlation. Correlation time was chosen to be 32,000 time steps (80 ps). According to a work on MD-based determination of the interfacial thermal conductance (Liang et al., 2013), one can determine the G_k by fitting the tail of the integration of the power auto-correlation function (PACF) by exponential functions. Five (5) other simulations were performed for the same structure with different initial conditions to check on the repeatability of the simulations.

Table 2-1: Summary of mathematical equations for the NERD force field

Bond stretching potential	$\frac{U(r)}{k_B} = \frac{k_r}{2}(r - b_{eq})^2$	$k_r = 96{,}500$ K/$Å^2$ $b_{eq} = 1.54$ $Å$
Bond bending potential	$\frac{U(\theta)}{k_B} = \frac{k_\theta}{2}(\theta - \theta_{eq})^2$	$k_\theta = 62{,}500$ K/rad^2 $\theta_{eq} = 114°$
Torsional potential	$\frac{U(\psi)}{k_B} = U_0 + U_1(1 + \cos\psi) + U_2(1 - \cos 2\psi) + U_3(1 + \cos 3\psi)$	$U_0 = 0$ $U_1 = 355.04\ K$ $U_2 = -68.19\ K$ $U_3 = 701.32\ K$
k_B: $Boltzmann\ constant$ = $1.381 \times 10^{-23}\ JK^{-1}$ b_{eq}: $Equilibrium\ bond\ length$ = 1.54 $Å$ θ: $Bond\ angle$ θ_{eq}: $Equilibrium\ bond\ angle$ = 114°		

Table 2-2: Parameters of the Lennard-Jones model for pair potentials

CH_2-CH_2	$\sigma = 3.93\ \AA$ $\varepsilon = 0.0907\ kcal/mol$
CH_3- CH_3	$\sigma = 3.91\ \AA$ $\varepsilon = 0.2059\ kcal/mol$
CH_2-CH_3	$\sigma_{CH_2-CH_3} = \frac{\sigma_{CH_2} + \sigma_{CH_3}}{2}$ $\varepsilon_{CH_2-CH_3} = \left(\varepsilon_{CH_2}\varepsilon_{CH_3}\right)^{1/2}$

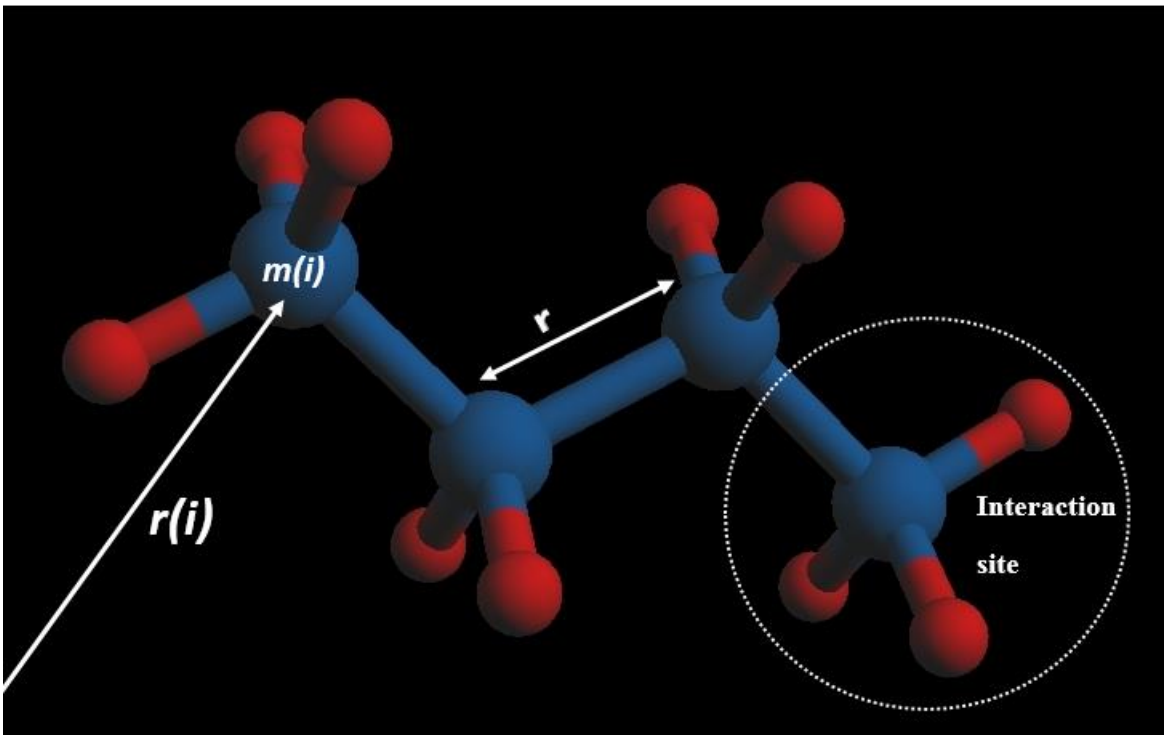

Figure 2-1: Schematic view of the interaction parameters in one n-alkane (Figure produced by ArgusLab software)

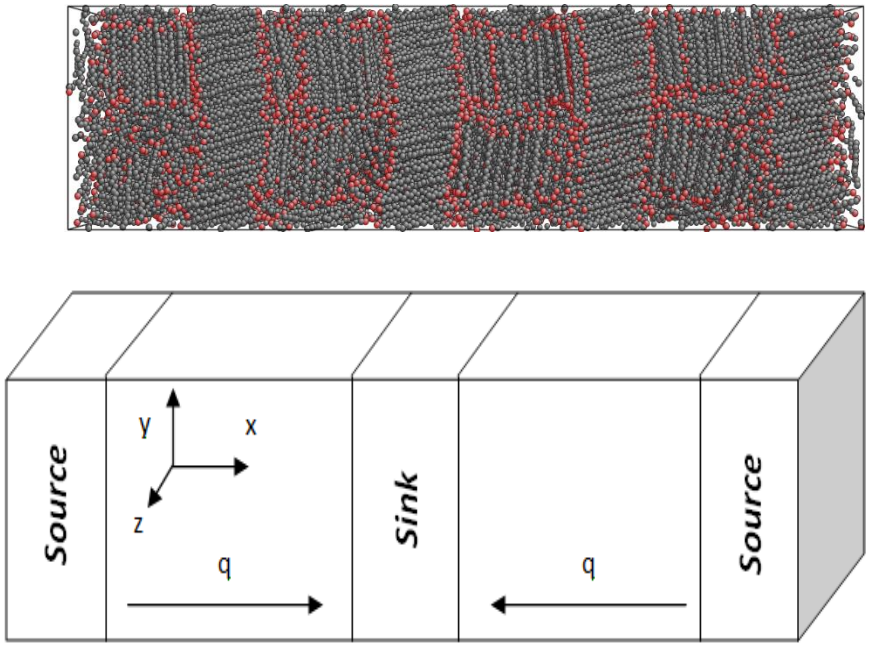

Figure 2-1: Schematic view of the position of the heat sink and sources in the system

3. Chapter 3: Thermal Conductivity of n-alkanes

3.1 Introduction

Phase change materials (PCM) have the great potential to be utilized in thermal energy storage/conversion systems, waste heat recovery, thermal management of electronics, etc. These materials can store thermal energy upon melting and then release the absorbed energy during freezing at a nearly constant temperature. This type of storing thermal energy is known as the latent heat mode of thermal energy storage. Among the 500+ materials known as PCM (some groups shown in Fig. 1.2), n-alkanes (C_nH_{2n+2}) in particular are the most commonly-used materials as PCM. N-alkanes exhibit small or no degree of supercooling in their melting and solidifying cycles and they have moderate thermal energy storage density. Compared to other types of PCM, n-alkanes exhibit low thermal conductivity. Great effort has been applied to improve the thermal conductivity of paraffin-based thermal energy storage systems (Fan and Khodadadi, 2011). For instance, introduction of high aspect-ratio nano-scale highly-conductive materials into n-alkanes to enhance the thermal conductivity has gained great interest in recent years (Wang et al., 2009). Great efforts have been devoted to investigate the crystalline structures that the n-alkanes possess in their solid form utilizing different methods such as the X-ray scattering, MD simulations and etc. In the literature, there are thermal conductivity data of shorter n-alkanes in both liquid and solid phases. However, as the number of carbon atoms within the molecule chains increase, thermal conductivity data on solid phase n-alkanes is missing. From the earlier studies it is well-known that for the shorter n-alkanes when the number of carbon atoms within the molecule chain is less than 20, the thermal conductivity of the n-alkanes increase in both solid and liquid phase as the length of the n-alkane molecule goes up. Therefore, we studied the effect of the length of the n-alkane molecules on their thermal conductivity for longer n-alkanes ($n > 20$).

This chapter is devoted to a discussion of both MD and experimental studies on the determination of the thermal conductivity of n-alkanes. Firstly, section 3.2 presents a short introduction on n-alkanes and their structure. This chapter continues with section 3.3 which is about MD simulations utilized to determine the thermal conductivity of the n-alkanes (n= 20, 24, 26 and 30).

In section 3.4, we utilized the transient plane source (TPS) method to measure the thermal conductivity of these n-alkanes (n= 20, 24 and 26). The TPS method has been widely used by researchers to measure thermal conductivity of a wide range of materials.

Thermal conductivity data from the MD simulations and the experiments are then compared in section 3.5.

3.2 N-alkanes

Normal alkanes, also called linear alkanes (C_nH_{2n+2}) that are widely known as Paraffins, are the most commonly-used materials as PCM. N-alkanes consist of hydrogen and carbon atoms with single bonds. Each carbon atom has four (4) bonds which can be either C-H or C-C bonds. N-Eicosane, for example, is a well-known n-alkane with 20 carbon atoms in the chain ($C_{20}H_{42}$) which is shown in Figure 3-1.

N-alkanes exhibit small or no degree of supercooling in their melting and solidifying cycles and they have moderate thermal energy storage density. These properties resulted in significant interest in applying n-alkanes to thermal energy conversion/storage devises as an ideal PCM. However, compared to other types of PCM, n-alkanes exhibit low thermal conductivity.

Different factors can affect the thermal conductivity of n-alkanes. Molecular structure, intramolecular structure and the interaction among the molecules and atoms are mainly

responsible for thermal transport within these molecules (Rastorguev et al., 1975). Other factors can also affect the thermal transport directly or by altering the above factors. In this thesis, the effect of the length of the n-alkane molecules on their thermal conductivity is investigated. The length of the molecule can be related to the mass of the molecule as well. Thus, the effect of either mass or the length of n-alkane molecules on the thermal conductivity is studied.

3.3 Molecular Dynamics Simulations

3.3.1 Review

There has been considerable effort to calculate the transport properties of n-alkanes utilizing the NEMD and EMD methods. Researchers have put great time and effort to calculate the shear viscosity of shorter n-alkanes (Edberg et al., 1987, Marechal et al., 1987). Babaei et al. (2013b) determined the thermal transport properties of n-eicosane using the NEMD and EMD simulations and predicted the thermal conductivity of n-eicosane in both liquid and solid phases. They realized that as the n-eicosane solidifies, the molecules form nano domain crystallines. They showed in their simulations that the thermal conductivity of solid phase n-eicosane is nearly twice the thermal conductivity of liquid n-eicosane and this enhancement is mainly due to the observed nanoscale grain boundaries. The effect of adding nano additives such as carbon nanotubes (CNT) and graphene sheets is investigated in their work as well (Babaei et al., 2013b). They utilized both NEMD and EMD simulations to determine the thermal interfacial conductance between the paraffin and CNT layers and paraffin and graphene sheets as well. Luo et al. (2010) studied the chain length effect for systems with different alkanedithiol molecule chain lengths using EMD simulations. They determined the thermal conductivity of 3 systems with different lengths that were -S-$(CH_2)_8$-S-, –S-$(CH_2)_9$-S- and –S-$(CH_2)_{10}$-S-. They believed that there is no chain length effect on the thermal conductivity based on their simulations.

However, it is stated that longer n-alkanes (n=14 to 20) exhibit two different trends for thermal conductivity values depending on if n (number of carbon atoms in the chain) is odd or even (Murashov and White, 2004). Moreover, it is stated that thermal conductivity of n-alkanes increases linearly as the number of the carbon atoms increase (Murashov and White, 2004). N-alkane molecules with an odd number of carbon atoms exhibit 30% lower thermal conductivities compared to the molecules with an even number of carbon atoms. This behavior is mainly because of the different packing structures at low temperatures which is called polymorphism (Ryckaert and Klein, 1986). Polymorphism of n-alkanes can be described in the way that molecules with odd (n-odd alkanes) and even (n-even alkanes) numbers of carbon atoms exhibit different crystal structures at low temperatures in their solid phase. In effect, different trends for the thermodynamic properties of odd and even n-alkanes, such as the equilibrium melting point and also thermal conductivity of n-alkanes are observed. Moreover, n-even alkanes exhibit a degree of supercooling of more than 3 °C which are not observed in n-odd alkanes phase diagrams. Between low-temperature highly-ordered solid structures and the liquid phase, there exist a series of weakly-ordered crystalline phases near the melting point which are called "rotator (R) phases" (Ungar and Masic, 1985). To date, five (5) different R-phases for n-alkanes have been identified. In the previous studies, different thermodynamic behaviors of n-alkanes were related to the existence of different rotator phases (R-phases) right before melting. R-phases are a series of phases that occur between the fully-ordered crystalline phases of n-alkanes and the liquid phase without any long range order about their long axis. For instance, it is believed that the presence of the R-phase at the surface near the crystallization point can serve as an ideal nucleation site for crystallization which can be the reason behind the lack of supercooling in n-odd alkanes. Sirota et al. (1992) presented a detailed study on the rotator phases of n-alkanes

using the x-ray scattering technique. However, MD simulations have also been utilized to study theses rotator phases.

Ryckaert et al. (1987) used MD simulations to investigate the rotator phase structures and the effect of temperature on packing within the n-odd n-alkanes chains. They utilized a centered orthorhombic lattice for the initial structure of the n-alkanes. The phase change of different n-alkanes from butane to n-dodecane was studied by Esselink et al. (1994) utilizing MD simulations. They determined the melting and crystallization temperatures for those n-alkanes. Marbeuf and Brown (2006) studied the transition from ordered crystalline to a melt for odd and even n-alkanes ($C_{18}H_{38}$, $C_{19}H_{40}$, and $C_{20}H_{42}$) using MD calculations. Based on the number of carbons and whether it is odd or even, alkanes show different behaviors in melting process in terms of rotator phases before complete melting. Wentzel and Milner (2010) carried out MD simulation to study the ordered rotator phases of pure C_{23} and a mix of C_{21}-C_{23}. They tried different all-atom potentials for the n-alkane molecules and showed that their results were in good agreement with the observed physical properties measured by experiments.

Rao et al. (2013) utilized MD simulations to investigate the self-diffusion and heat capacity of n-alkanes and their binary mixtures. Two n-alkanes including n-nonadecane ad n-tetracosane and their mixtures were used in this study. They compared the results of their MD simulations with the experimental observations.

In this thesis, effect of the length of the n-alkane molecules on their thermal conductivity is investigated. For this objective, four (4) n-alkane molecules with different lengths are studied. $C_{20}H_{42}$ (n-eicosane), $C_{24}H_{50}$ (n-tetracosane), $C_{26}H_{54}$ (n-hexacosane) and $C_{30}H_{62}$ (n-triacontane) are the n-alkane molecules that are investigated in this work.

3.3.2 Simulation Methodology

The NEMD direct method has been used to determine the thermal conductivity of n-alkane molecules in liquid, solid and perfect crystal phases (Schelling et al., 2002). In the direct method, a known heat flux is imposed through the simulation box. The heat flux can be generated by exchanging kinetic energy between cold (sink) and hot (source) slabs. The thermal conductivity can then be determined using the Fourier's law under steady state conditions.

$$q_i = -k_{ij} \frac{dT}{dX_j}, \tag{3.1}$$

where q_i (i =1, 2 and 3) is the heat flux component in the *i*-th direction, k_{ij} is thermal conductivity tensor and $\frac{dT}{dX_j}$ is the temperature gradient due to the heat flux. This approach was adopted in view of the negligible effect of the anisotropy for solid systems (Appendix A).

Interaction between atoms of n-alkane molecules is defined by the NERD force field (Nath et al., 1998). Neighboring atoms, bonds, angles and dihedrals are required to be defined in the appropriate input file to utilize this potential. This force field describes bonded interactions with bond stretching, bending and torsion and non-bonded interactions with the LJ potential between the interaction sites within different molecules and with the appropriate cut-off radius for the sites in the same molecules.

The Newton's equations of motion are integrated numerically using the velocity Verlet algorithm with a time step of 1 fs. All simulations were performed with the large-scale atomic/molecular massively parallel simulator (LAMMPS) molecular dynamics package (Plimpton, 1995).

3.3.3 Model Structures

3.3.3.1 Bulk structures

Four different n-alkanes including $C_{20}H_{42}$, $C_{24}H_{50}$, $C_{26}H_{54}$ and $C_{30}H_{62}$ (n=20, 24, 26 and 30) are the molecules with different lengths that were studied in this work. In each case, the simulated system contains 600 molecules of each of these n-alkanes which were created using the Packmol package (Martínez et al., 2009). The systems were initially equilibrated under the NPT conditions at 360 K and atmospheric pressure for 5,000,000 time steps. Molecules in the liquid phase for the case of $C_{24}H_{50}$ were observed to be oriented randomly as shown in Figure 3-2. The systems were then cooled down to T = 230 K at a rate of 1.5 K/ns to obtain the solid structures and Figure 3-3 exhibits the typical structures of the realized solid phase after freezing for the case of $C_{24}H_{50}$. Molecules in the solid case exhibit a localized ordering with the grain boundaries of paraffin molecules aligned in different directions. This alignment is a reason for the higher thermal conductivities compared with the liquid phase. The solid structure was heated up to 360 K again and the re-melt process was performed. The change in the potential energy of the systems during the solidification and re-melting process for the case of $C_{24}H_{50}$ is given in Figure 3-4. Observing an abrupt change in the potential energy is an indication of crystallization and melting temperatures. As shown in this figure, the melting temperature is different from the crystallization temperature and this can be caused by the purity of the system. Molecules cannot crystallize at melting temperatures since solidification is in need of a nucleation site and it is difficult for the molecules in pure systems to nucleate. This phenomenon is called supercooling which is well-known (Chalmers, 1959, and Knight, 1967).

To consider the effect of the orientation of the chains with respect to the direction of the imposed heat flux, we computed the alignment factor (s) to determine how the thermal conductivity

changes with alignment of the molecules (Rigby and Roe, 1988). The alignment factor is given by:

$$s = \left| \frac{\langle \cos^2 \theta \rangle - \frac{1}{3}}{\frac{2}{3}} \right|, \quad (3.2)$$

where Θ is the angle between the end-to-end vector of each molecule and the desired axis with the symbol < > standing for the average over all molecules. The alignment parameter can vary from 0 to 1 with the limits corresponding to completely random orientation of the molecules and the molecules perfectly aligned along the desired direction, respectively.

3.3.3.2 Perfect Crystal

Perfect crystal is an idealized model for which all the molecules will be aligned in one direction and it can be used as a reference model which gives the maximum possible thermal conductivity of these molecules along the molecular axis. Four different n-alkanes including $C_{20}H_{42}$, $C_{24}H_{50}$, $C_{26}H_{54}$ and $C_{30}H_{62}$ were chosen for this study. The basic unit of these structures included 161 molecules which resulted in the same surface area for the simulation boxes for all the cases. The Xenoview© software (Shenogin and Ozisik, 2007) was used to align the molecules in a hexagonal lattice. Xenoview is a MD program that is used for creating structures with a built-in graphical user interface. Figure 3-5 exhibits the structure developed using Xenoview© for the case of $C_{20}H_{42}$. The system was then equilibrated under the *NPT* conditions at T = 150 K and atmospheric pressure for 5,000,000 time steps and then heated up to T = 270 K for another 5,000,000 time steps and was equilibrated at T = 270 K under the *NPT* conditions over 3,000,000 time steps. Figure 3-6 shows a snapshot of the realized system for the $C_{20}H_{42}$ molecules after equilibration and Figure 3-7 is the corresponding snapshot of the stacked system composed of 12 replications.

3.3.4 Results

Temperature profiles associated with the imposed heat flux for the liquid systems are shown in Figure 3-8 for the four n-alkanes systems studied. The value of the heat flux for the case of bulk liquid was set to be 0.01 kcal/mol. Based on the average temperature gradients and the heat flux, the thermal conductivity of liquid modes was determined and tabulated in table 3-1. Figure 3-9 exhibits the trend for the computed values of the thermal conductivity of liquid n-alkanes with the number of carbon atoms in the chain and compares these values with the experimental data of Rastorguev et al. (1974) for liquid n-alkanes (n less than or equal to 24). The MD-predicted values of the thermal conductivity exhibit the same trends of the experimental data in liquid phase, i.e. the thermal conductivity rises as the chain length is increased.

Thermal conductivity of the solid n-alkanes was determined as well. There is a strong possibility that the thermal conductivity within the structures is not isotropic. Thus, thermal conductivity was determined in three (3) spatial directions (xx-, yy- and zz- components of thermal conductivity matrix). To address the possible size effect, the base structure was replicated along the heat current direction for four (4) to twelve (12) times. The associated computed thermal conductivity values of the molecules are plotted in Figure 3-10 for different number of replicas. Table 3-2 summarizes all the computed thermal conductivity values in the x-, y- and z-directions. Note that in extracting the thermal conductivity of the materials from Figure 3-10 following the procedure outlined in Chapter 2, some data for higher replicas were eliminated in order to consider the possible size effect. Results of table 3-2 exhibit a weak dependence of the thermal conductivity on direction. The trend for variation of the thermal conductivity (averaged over x-, y- and z-components) of the solid structures with the length of the molecule is shown in

Figure 3-11. The results of the MD simulations suggest that the thermal conductivity in solid phase rises as the chain length is increased.

In order to determine the thermal conductivity of the perfect crystal phase of n-alkanes, the base structures were replicated in the molecular axis direction for 6, 8, 10, 12 and 14 times to investigate the size effect of the simulation box. The systems then were equilibrated under the NVT conditions for 3,000,000 time steps when the systems attained steady state. The NVT ensemble was chosen over the NPT ensemble because under the *NPT* conditions the layers are pushed toward each other and the structure is not perfect anymore. The value of the heat flux was chosen to be 0.005 kcal/mol and imposed over the system for 5,000,000 time steps. The resulting temperature profiles for perfect crystal stacked structures are shown in Figure 3-12 for the various n-alkanes studied. Temperature profiles were averaged over the last 1,000,000 time steps of heat flux addition. The temperature profiles in Figure 3-12 exhibit distinct stepwise behavior wherein the temperature drops/rises occur essentially at the interfaces between the crystalline layers of n-alkanes. Within each layer, the temperature profile is almost flat due to the ballistic phonon transport along straight alkane chains (Chen, 2000). For each case, thermal conductivity of the replicated system was evaluated utilizing the associated temperature profiles. Inverse of the computed thermal conductivity values was plotted versus the inverse of the length of the various n-alkanes structure as shown in Figure 3-13. The length-independent thermal conductivity of each molecule was determined by fitting the individual graphs in Figure 3-13 by an appropriate linear function. The thermal conductivity values for the perfect crystal structures are tabulated in Table 3-3 and plotted in Figure 3-14. The results of the MD simulations suggest that the thermal conductivity of the perfect crystal structures rises as the chain length is increased.

3.4 Experimental Measurement

3.4.1 Literature review

Rastorguev et al. (1974) measured the thermal conductivity of long n-alkanes at different temperatures for liquid phases experimentally using the heated-filament technique. They showed that the thermal conductivity in the liquid phase decreases linearly as the temperature of the sample is increased. They also stated that their experiments exhibited a rise in thermal conductivity in the liquid phase as the number of carbon atoms in the chain is raised (Figure 3-9). They believed that n-alkanes follow no trend of direct proportionality with the number of carbon atoms and the reason was that the thermal conductivity of n-alkanes showed an asymptotic behavior as the number of carbon atoms increase and finally the value of the thermal conductivity approaches an asymptotic value as the molecular length becomes high.

Yarbrough and Kuan (1981) did some experiments using a radial heat flow apparatus to determine the thermal conductivity of n-alkanes in the solid phase and they asserted that the thermal conductivity has an inverse relation with temperature that lead to a linear decrease of thermal conductivity as temperature rises. Moreover, they showed that the thermal conductivity values of the n-even alkanes are higher than those with an odd number of the carbon atoms in the chain. There is a linear increase of thermal conductivity with the number of carbon atoms (Figure 3-20).

Stryker and Sparrow (1989) used a spherical thermal conductivity cell operating under steady state condition to determine the thermal conductivity of solid n-eicosane as a function of sample mean temperature, rate of solidification and some other parameters. They stated that despite the

results of Yarbrough and Kuan (1981), their experiments showed no temperature dependence for thermal conductivity values.

Yaws (1995) also reported thermal conductivity data for a wide range of organic compounds. He reported this data for n-alkanes (n = 8 to 28) mainly in liquid phase for higher n-alkanes.

Nabil (2013) (also Nabil and Khodadadi, 2013) utilized the transient plane source (TPS) method to measure the thermal conductivity of solid n-eicosane. They showed that the thermal conductivity of solid n-eicosane does not change significantly with temperature and it remains constant at different temperatures in the solid phase. Fang et al. (2013) basically repeated the experiments of Nabil (2013) for the solid n-eicosane using the TPS method and obtained the same results for the thermal conductivity.

3.4.2 Sample Preparation

Details of the preparation schemes of the NePCM liquid and solid samples are discussed in the theses of Fan (2011) and Nabil (2013), respectively. Similar steps for preparation of samples were followed in this study. N-eicosane ($C_{20}H_{42}$), n-tetracosane ($C_{24}H_{50}$) and n-hexacosane ($C_{26}H_{54}$) were selected as PCM. All of these samples were provided as 99% pure n-alkanes by Acros Organics (Thermo Fisher Scientific, Hampton, New Hampshire). Table 3-4 provides information about the physical properties of these n-alkanes. Firstly, the n-alkanes were weighed and melted followed by rigorous stirring on a hot-plate magnetic stirrer (SP131325Q, Thermo Fisher, Dubuque, IA) at 80 °C for 30 minutes.

The liquid samples then were placed inside a vacuum oven (Fischer Scientific, Isotemp® Vacuum Oven Model 281A) for at least 20 hours. The vacuum oven was operated at -30 kPa absolute pressure at a fixed temperature of 65 °C in order to degas the samples. The aluminum

molds were machined disks with a diameter of one inch and height of 0.375 inches. Commercial aluminum foil molds (VWR® International LLC, Model 611-1362) with a diameter of 1 inch was pressed into the machined aluminum molds using a custom-designed molding handle. Samples were solidified using the oven solidification method (Nabil, 2013) while the oven was turned off and maintained at the atmospheric pressure. The solidification process took 4 hours to be completed for all the samples. A photograph of the pure solid samples is shown in Figure 3-15 that shows sides of the solid disks of which was exposed to the local atmosphere. The weight of each sample was in the range of 3-4 grams. A brief overview diagram containing the descriptions of the preparation schemes is shown in Figure 3-16.

3.4.3 Experimental Details

The transient plane source (TPS) technique is known as the commonly-used transient method of measuring the thermal conductivity. The main advantage of the transient methods is that the measurement process is fast and extremely suitable for liquid samples measurements so as to avoid possible initiation of natural convection within the samples.

In this thesis, we utilized a Hot Disk Thermal Constants Analyzer system (TPS 500, Hot Disk AB, Gothenburg, SWEDEN) based on the transient plane source technique (maximum uncertainty of 2% specified by the manufacturer) to measure the thermal conductivity of solid n-alkanes samples.

Measurements were performed for a range of temperature varying from 0 ºC to temperatures just below the melting temperature of each sample. The two solid disks were positioned on a pair of aluminum cold plates (LYTRON Co., Woburn, MA, Model CP20G01), whereas the flow inlets and outlets of the cold plates (I.D. of 5/16 inches and O.D. of 3/8 inches) were connected to a

bath/circulator. The programmable temperature bath (TC-502P, Brookfield, Middleboro, MA) was utilized to circulate a 50:50 water/ethylene glycol solution as the working fluid at a constant temperature through the two cold plates. The bath system has a stability of 0.01 °C allowing the user to control the measurement temperature of interest within the bath. Due to the internally criss-crossed finned arrangement of the aluminum cold plates, the cold plates can be adjusted rapidly to the temperature of the bath. The sample-holding assembly was insulated effectively from the laboratory environment using Styrofoam® sheets. The temperature of solid discs were measured by the thermistor (GE, Model A733F-CSP60BT103M, accuracy of 0.01 °C) placed on top of the cold plate. An adjustable screw was used on top of a compression metal plate to impose a uniform pressure on the sample-holding assembly. Two adjustable screws on the sides of the set-up in addition to an adjustable metal plate were utilized to precisely adjust the horizontal level of the TPS sensor between the solid samples as recommended by the manufacturer. A schematic view of the measurement system is shown in Figure 3-17.

3.4.4 Results

For each pair of the solid samples, five sets of experiments were performed at a specific temperature to measure the thermal conductivity.

Thermal conductivity values for the three n-alkanes are shown in Figure 3-18 as a function of sample temperature and tabulated in Table 3-5. The measured thermal conductivity values for n-eicosane are in agreement with the experimental values reported by Stryker and Sparrow (1989) and Nabil (2013). Similar to Stryker and Sparrow (1989), no temperature dependence for thermal conductivity of these n-alkanes was observed in our work. Thermal conductivity values for the n-eicosane from our experiments are compared with the reported values of Nabil (2013) in Figure 3-19.

3.5 Comparison between Simulations and Experimental Observations

A comparison between the MD-predicted values of thermal conductivity and those from experiments is made in Figure 3-20. As is shown in Figure 3-20, MD simulations exhibit that the thermal conductivity increases very slightly as the number of carbon atoms within the n-alkanes chains goes up. However, our experiments are showing that thermal conductivity decreases as the length of the n-alkanes molecule increases. We know that the solidification process for the MD simulations and experiments might be different in process. As discussed by Nabil (2013), thermal conductivity of n-eicosane is strongly dependent on the specific process of solidification. The rate of solidification can result in different crystalline structures and different thermal conductivity values. To study the effect of crystalline structures, we calculated the alignment factors for the solid n-alkane samples using equation (3.2) and the values are tabulated in Table 3-6. It can be inferred from the data that alignment factor values are nearly in the same range for almost all the cases except for some cases that exhibit different values and this had no direct effect on thermal conductivity values as can be seen in Table 3-6.

Another interesting fact is that Yarbrough and Kuan (1981) showed in their experiments that thermal conductivity of the solid n-alkanes increase as the number of carbon atoms changes from 14 to 20 (Figure 3-20). However, our experiments show that thermal conductivity of solid n-alkanes (n=20, 24 and 26) remains almost unchanged from n=20 to n=24 and decreases from n=24 to n=26. More work is needed to realize what is the reason for this behavior of n-alkanes, However, R-phases within n-alkanes might be a strong candidate for the reason behind this behavior.

Thermal conductivity trends for perfect crystal n-alkanes are also interesting to us. It can be inferred from the data for perfect crystal that thermal conductivity exhibits a zigzag trend as the

number of n-alkanes increase from n=20 to n=30. As was discussed earlier, n-alkanes exhibit the same zigzag trend for some other thermodynamics properties such as melting temperature and etc. Since we don't have experimental data on thermal conductivity of solid n-triacontane (n=30), we cannot conclude that experiments exhibit the same zigzag trend for thermal conductivity or not.

3.6 Summary

Both MD simulations and experiments were utilized to determine the thermal conductivity of n-alkanes of interest. The direct method NEMD simulations is used to determine thermal conductivity of the n-alkanes (n=20, 24, 26 and 30) in liquid, solid and perfect crystal phase modes. Simulations exhibit that the thermal conductivity of the liquid n-alkanes increases as the number of carbon atoms within the chain rises. The solid phase n-alkanes exhibit a more organized structure than the liquid systems, where crystalline nano-domain structures are clearly seen in solid phases compared to randomly-oriented liquid systems. This suggests that as the structure gets more organized, it will result in higher thermal conductivity values. Moreover, it is shown that the perfect crystal structures exhibit higher thermal conductivities than solid systems. This can also be a proof to the fact that if the molecules in the system align in an organized structure, this will enhance the thermal conductivity. Experiments were used to measure the thermal conductivity of the n-alkanes (n=20, 24 and 26). Interestingly, experiments exhibit that as the length of the n-alkanes molecules increase, thermal conductivity of these n-alkanes decrease where MD simulations exhibit a very slight increase in the thermal conductivity as the number of carbon atoms within the chain increase. Moreover, perfect crystal n-alkanes follow a zigzag trend for thermal conductivity values with the number of carbon atoms within n-alkane molecules.

Table 3-1: MD-determined thermal conductivity values for liquid n-alkanes at T = 360 K and a comparison between these values with the available experimental data from Rastorguev et al. (1974)

N-alkane	n-eicosane $C_{20}H_{42}$	n-tetracosane $C_{24}H_{50}$	n-hexacosane $C_{26}H_{54}$	n-triacontane $C_{30}H_{62}$
Thermal conductivity (W/m K) Present work (MD) T = 87 °C	0.154	0.162	0.167	0.191
Experiments Rastorguev et al. (1974) T = 100 °C	0.1341	0.1426	-	-

Table 3-2: MD-determined thermal conductivity values for solid n-alkanes at T=270 K

N-alkane		n-eicosane $C_{20}H_{42}$	n-tetracosane $C_{24}H_{50}$	n-hexacosane $C_{26}H_{54}$	n-triacontane $C_{30}H_{62}$
Thermal conductivity (W/m K)	X-component	0.41	0.35	0.44	0.53
	Y-component	0.40	0.47	0.41	0.39
	Z-component	0.35	0.36	0.38	0.40

Table 3-3: MD-determined thermal conductivity values for perfect crystal n-alkanes at T = 270 K

N-alkane	n-eicosane $C_{20}H_{42}$	n-tetracosane $C_{24}H_{50}$	n-hexacosane $C_{26}H_{54}$	n-triacontane $C_{30}H_{62}$
Thermal conductivity (W/m K)	0.86	0.92	0.86	1.05
Standard deviation for curve fitting	0.4054	0.0768	0.489	0.5755

Table 3-4: Physical properties of the n-alkanes supplied by ACROS ORGANICS (Thermo Fisher Scientific, Hampton, New Hampshire)

N-alkane / Property	n-eicosane $C_{20}H_{42}$	n-tetracosane $C_{24}H_{50}$	n-hexacosane $C_{26}H_{54}$
Density (g/mL)	0.7886	0.797	0.8
Melting point (°C)	36-38 °C	49-52 °C	56-59 °C
Boiling point (°C)	220 °C	391 °C	420 °C
Solubility in Water	Insoluble	Insoluble	Insoluble

Table 3-5: Thermal conductivity data for solid n-eicosane, n-tetracosane and n-hexacosane samples at different temperatures using the oven solidification method; Data are averaged over five measurements (maximum standard deviation of 1%)

N-alkane		n-eicosane $C_{20}H_{42}$	n-tetracosane $C_{24}H_{50}$	n-hexacosane $C_{26}H_{54}$
Thermal conductivity (W/m K)	0 ºC	0.4465	0.4433	0.3929
	5 ºC	0.4444	0.4594	0.3776
	10 ºC	0.4436	0.4384	0.3698
	15 ºC	0.4366	0.4354	0.3840
	20 ºC	0.4309	0.4353	0.3663
	25 ºC	0.4357	0.4339	0.3780
	30 ºC	0.4315	0.426	0.3712
	35 ºC	-	0.4151	0.3717

Table 3-6: Alignment factors in 3 spatial directions for solid n-alkanes from MD simulations and the effect of alignment on the thermal conductivity of the solid samples

N-alkane		n-eicosane $C_{20}H_{42}$	n-tetracosane $C_{24}H_{50}$	n-hexacosane $C_{26}H_{54}$	n-triacontane $C_{30}H_{62}$
Alignment factor	X-dir.	0.44	0.26	0.27	0.16
	Y-dir.	0.19	0.27	0.29	0.30
	Z-dir.	0.11	0.22	0.19	0.29
Thermal Conductivity (W/m K)	X-dir.	0.37	0.35	0.44	0.41
	Y-dir.	0.40	0.47	0.41	0.39
	Z-dir.	0.35	0.36	0.34	0.40

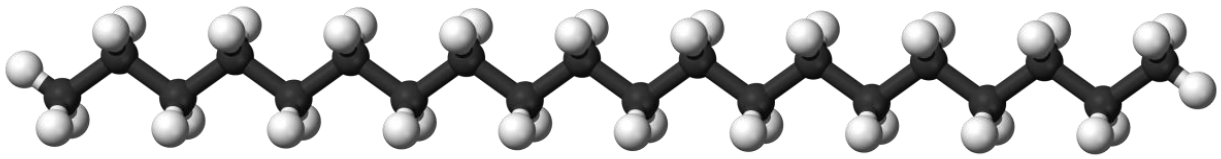

Figure 3-1: N-eicosane ($C_{20}H_{42}$) molecule structure (dark grey balls represent carbon atoms and light grey balls are hydrogen atoms)

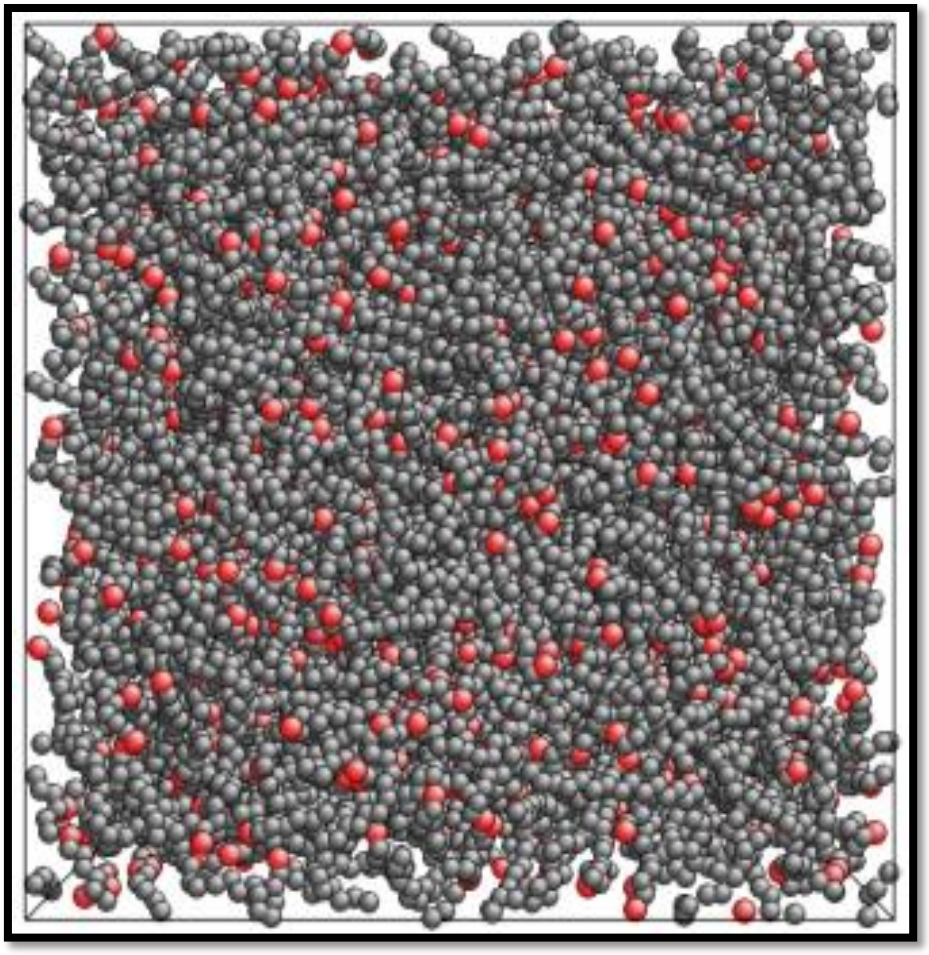

Figure 3-2: Snapshot of the system in the liquid phase after equilibration for $C_{24}H_{50}$ molecules (red balls shown as $-CH_3$ groups and dark balls as $-CH_2-$ groups)

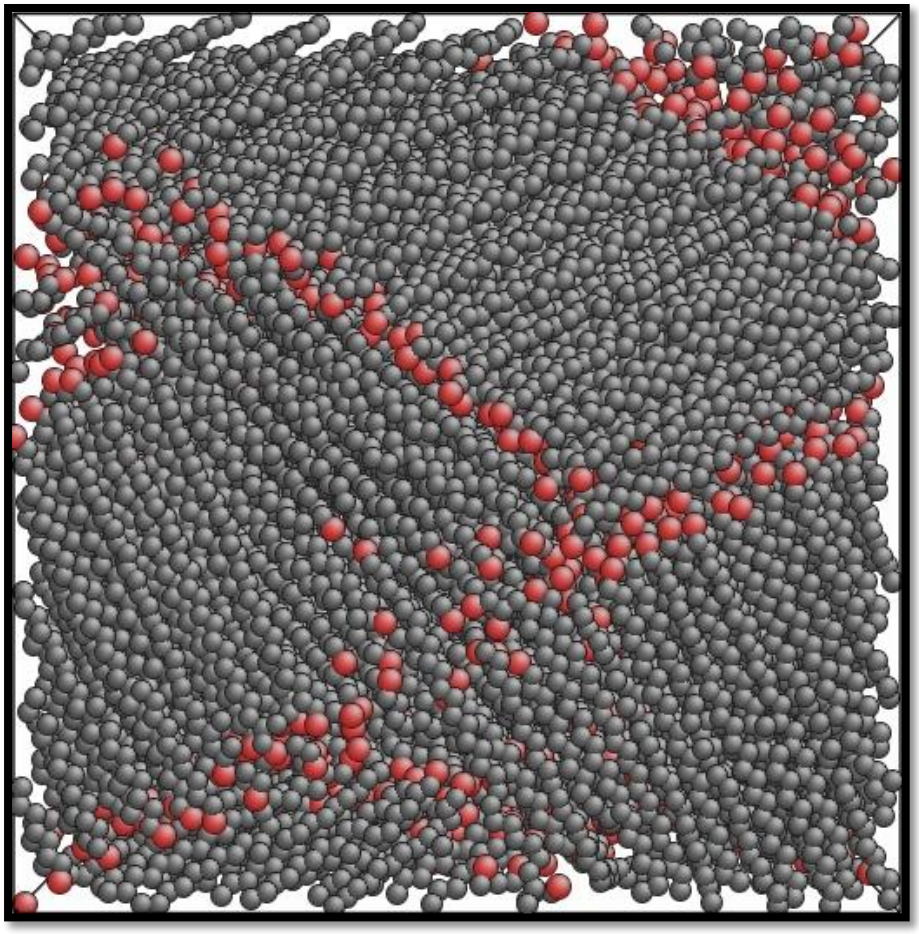

Figure 3-3: Snapshot of the system in the solid phase after equilibration for $C_{24}H_{50}$ molecules (red balls shown as $-CH_3$ groups and dark balls as $-CH_2-$ groups)

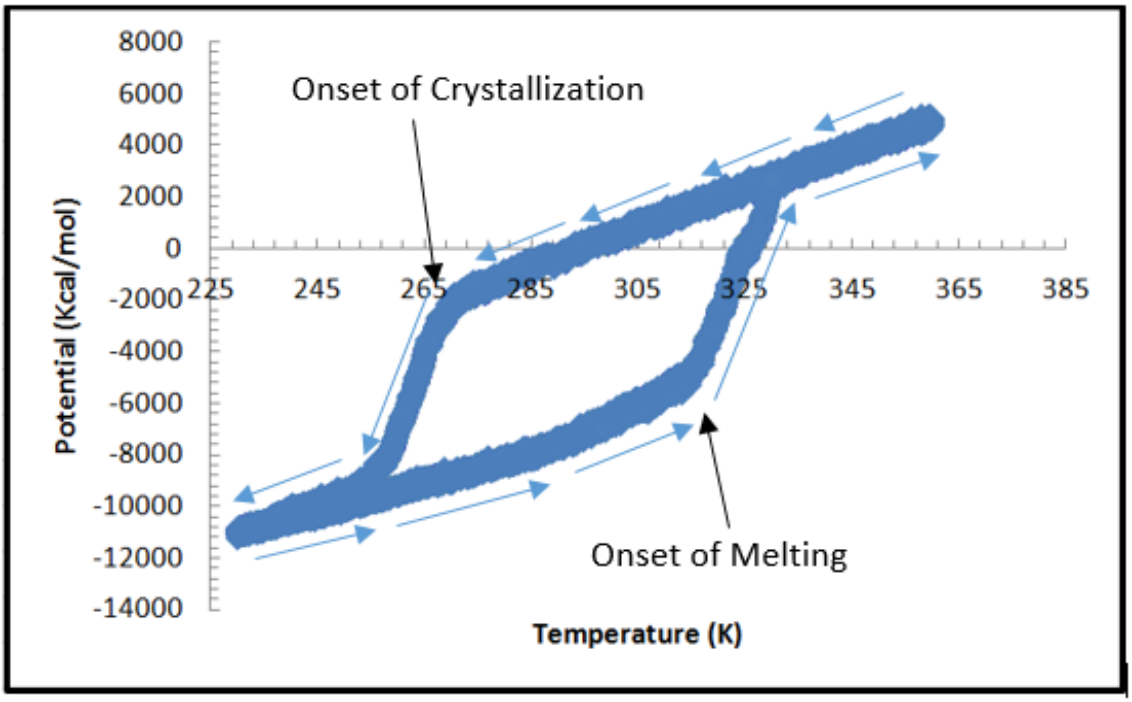

Figure 3-4: Potential energy change during the melting-solidification cycle for $C_{24}H_{50}$

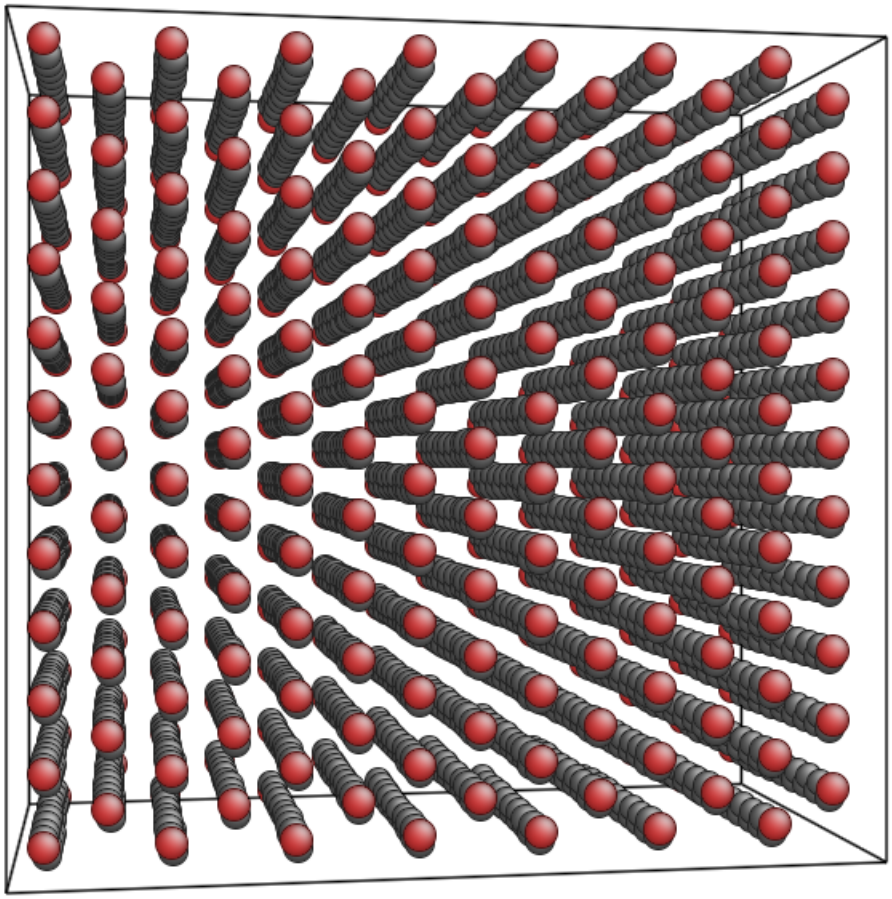

Figure 3-5: Snapshot of the perfect crystal model structure before equilibration for the $C_{20}H_{42}$ molecules

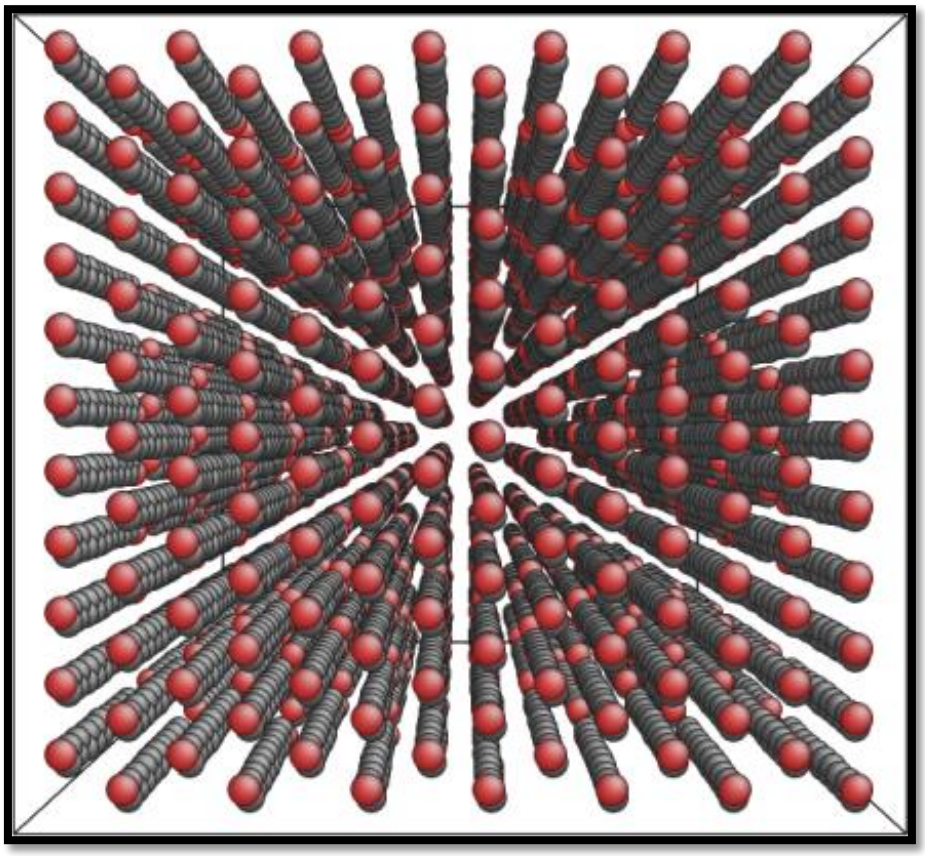

Figure 3-6: Snapshot of the equilibrated system of the $C_{20}H_{42}$ molecules for the perfect crystal model

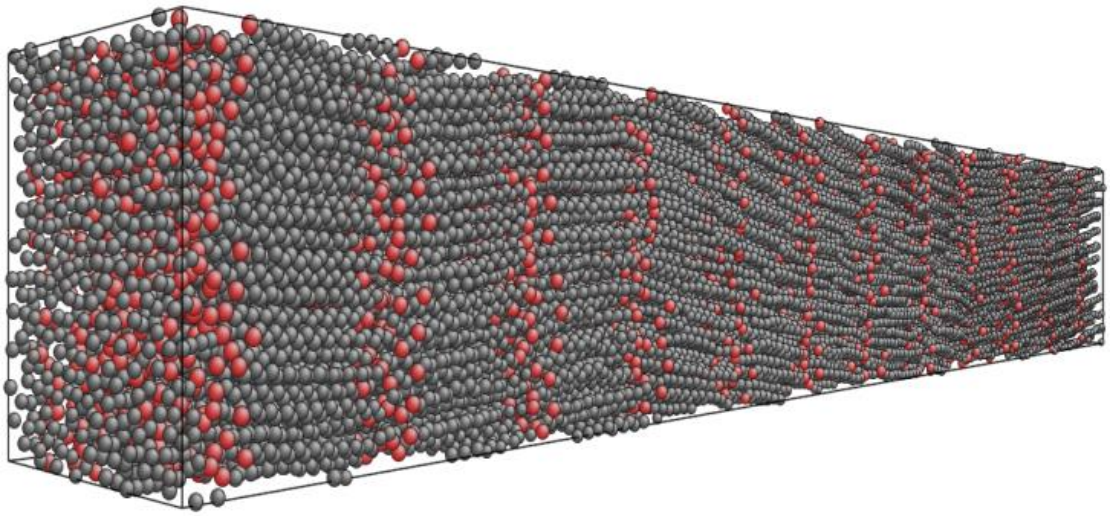

Figure 3-7: Snapshot of the stacked system of 12 replicas for the perfect crystal of $C_{20}H_{42}$

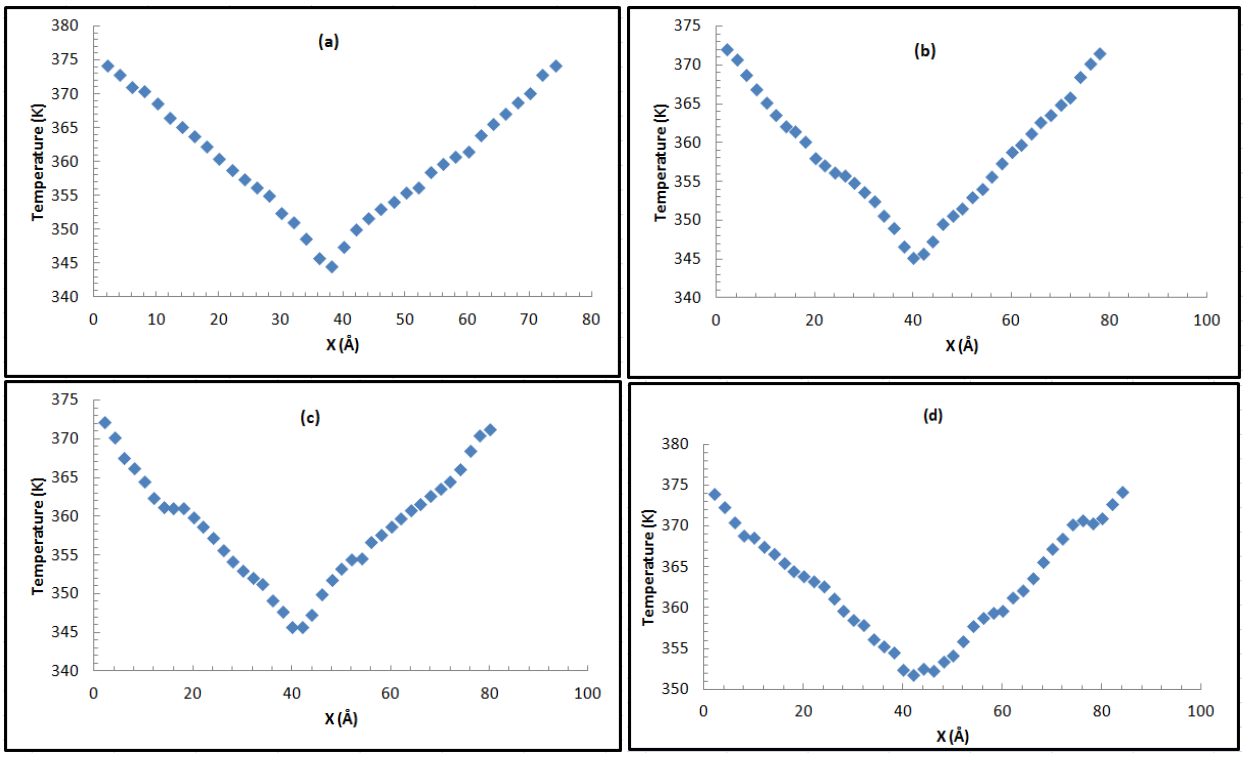

Figure 3-8: Temperature profiles in response to the imposed heat flux for liquid phases of (a) $C_{20}H_{42}$, (b) $C_{24}H_{50}$, (c) $C_{26}H_{54}$ and (d) $C_{30}H_{62}$

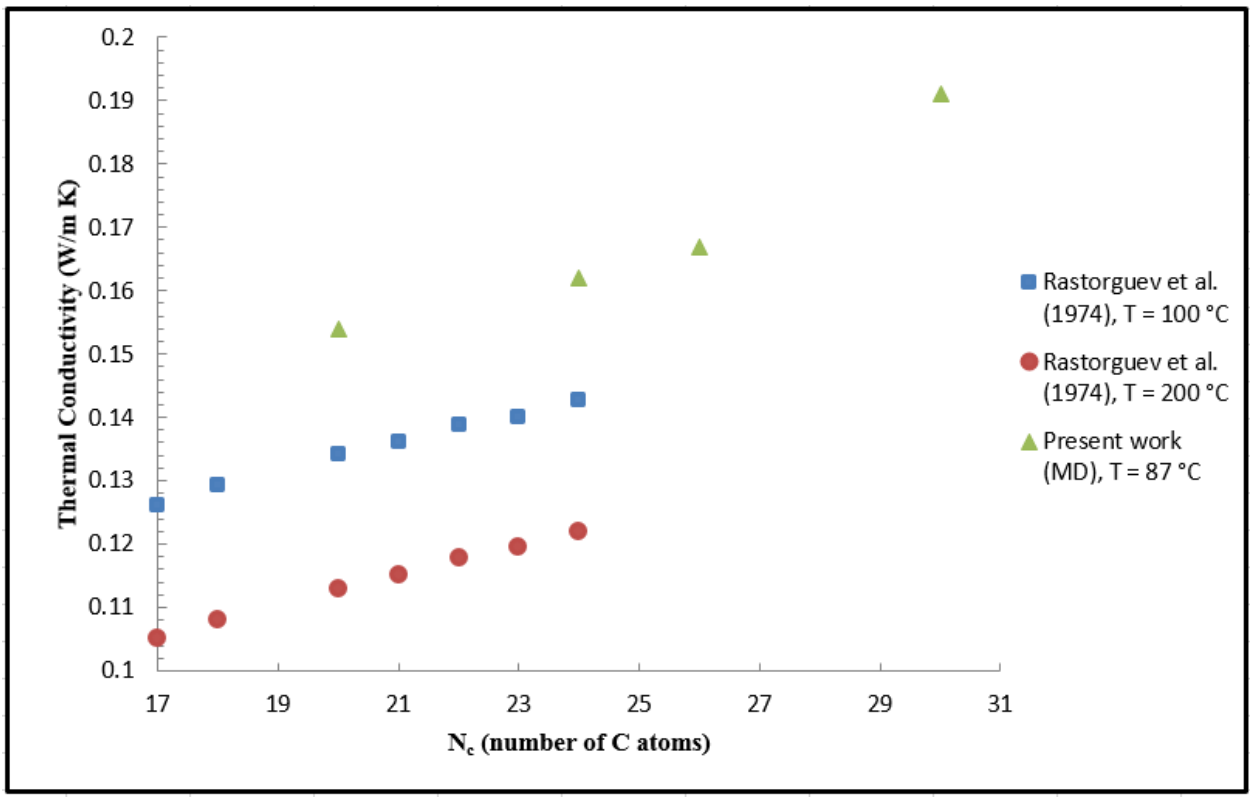

Figure 3-9: MD-determined thermal conductivity values for liquid n-alkanes at T = 360 K versus the number of carbon atoms within the chain compared with the experimental data from Rastorguev et al. (1974)

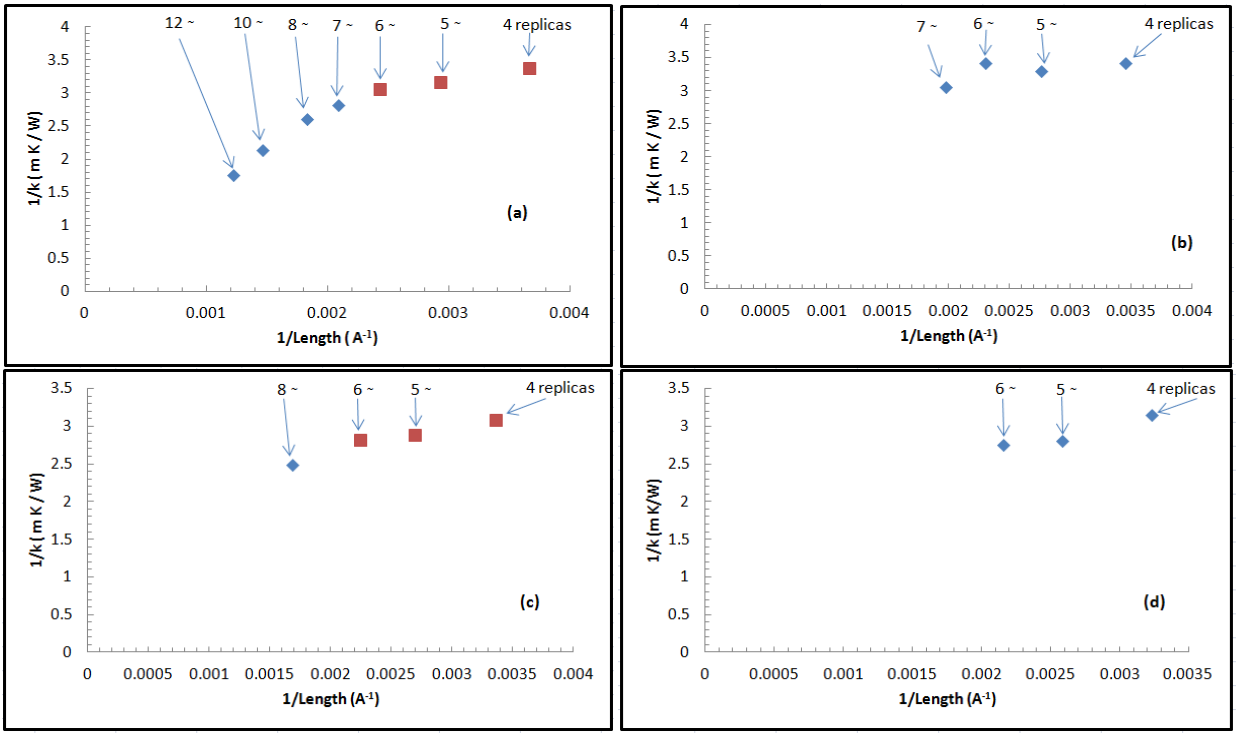

Figure 3-10: Inverse of the thermal conductivity in the x-direction versus the inverse of the length of the stacked layers for different number of replicas for solid (a) $C_{20}H_{42}$, (b) $C_{24}H_{50}$, (c) $C_{26}H_{54}$ and (d) $C_{30}H_{62}$

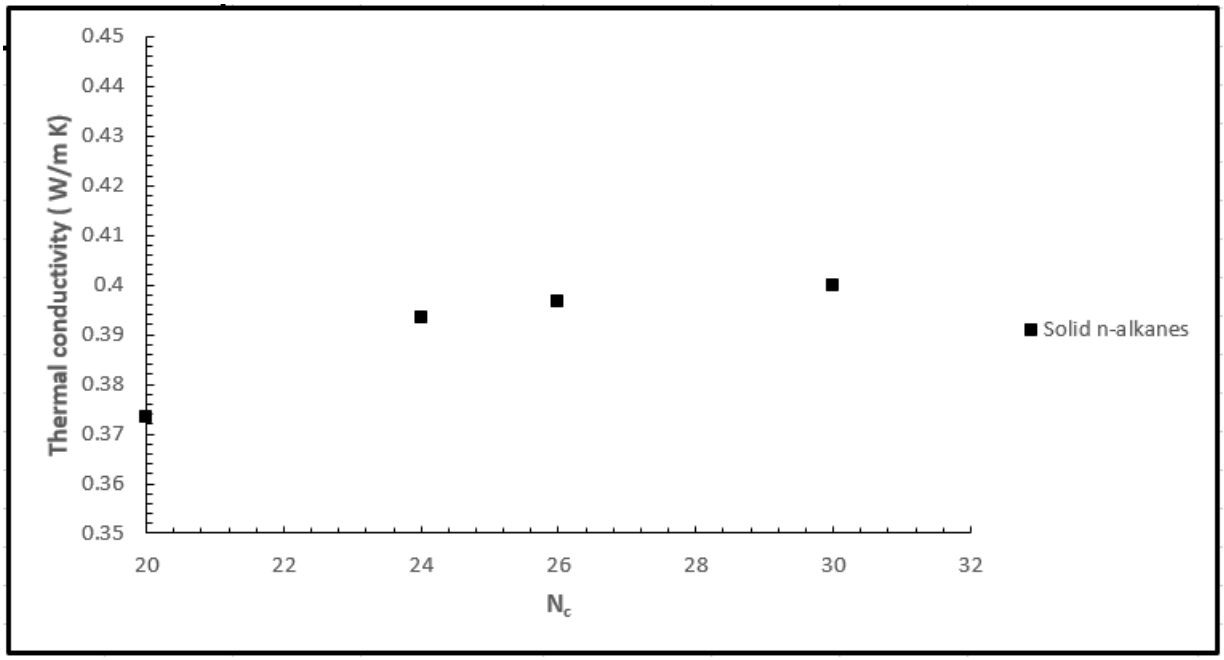

Figure 3-11: MD-determined thermal conductivity values (averaged over all three spatial directions) for solid n-alkanes at T = 270 K versus the number of carbon atoms within the chain

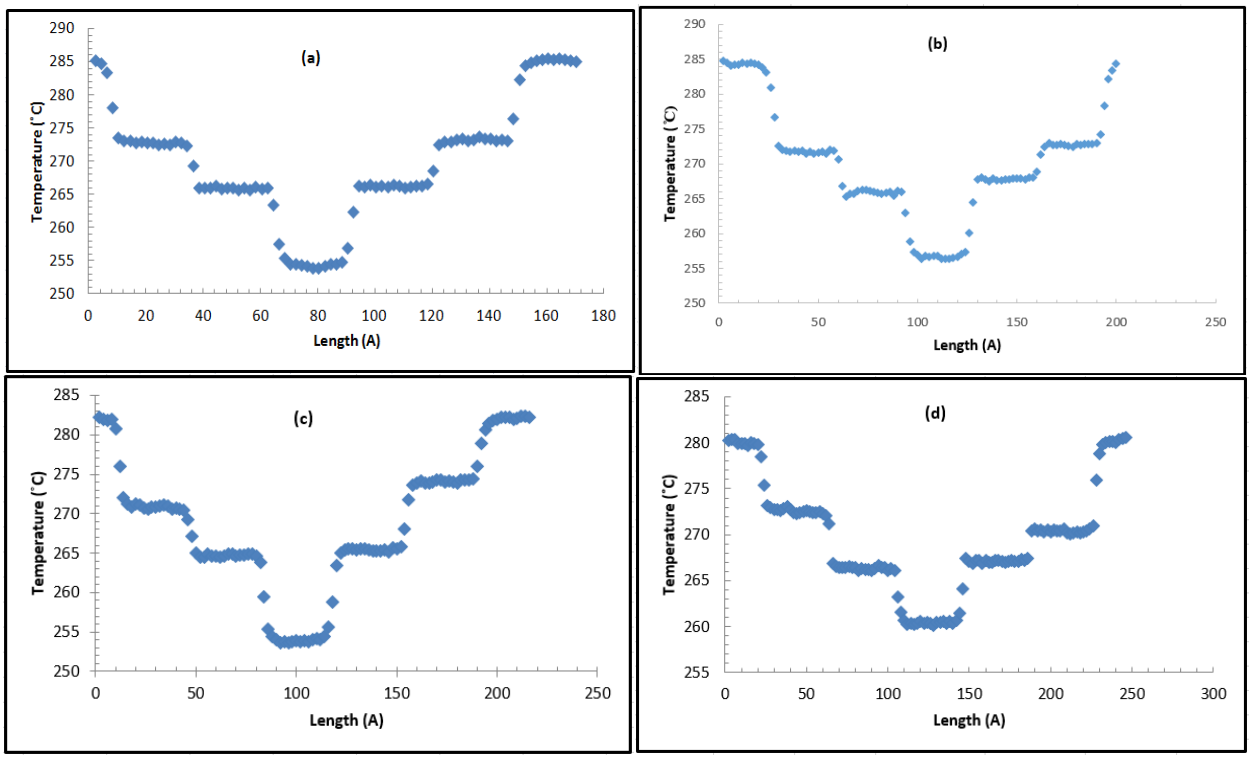

Figure 3-12: Temperature profiles for the case of perfect crystals with six (6) replications in response to the imposed heat flux for (a) $C_{20}H_{42}$, (b) $C_{24}H_{50}$, (c) $C_{26}H_{54}$ and (d) $C_{30}H_{62}$

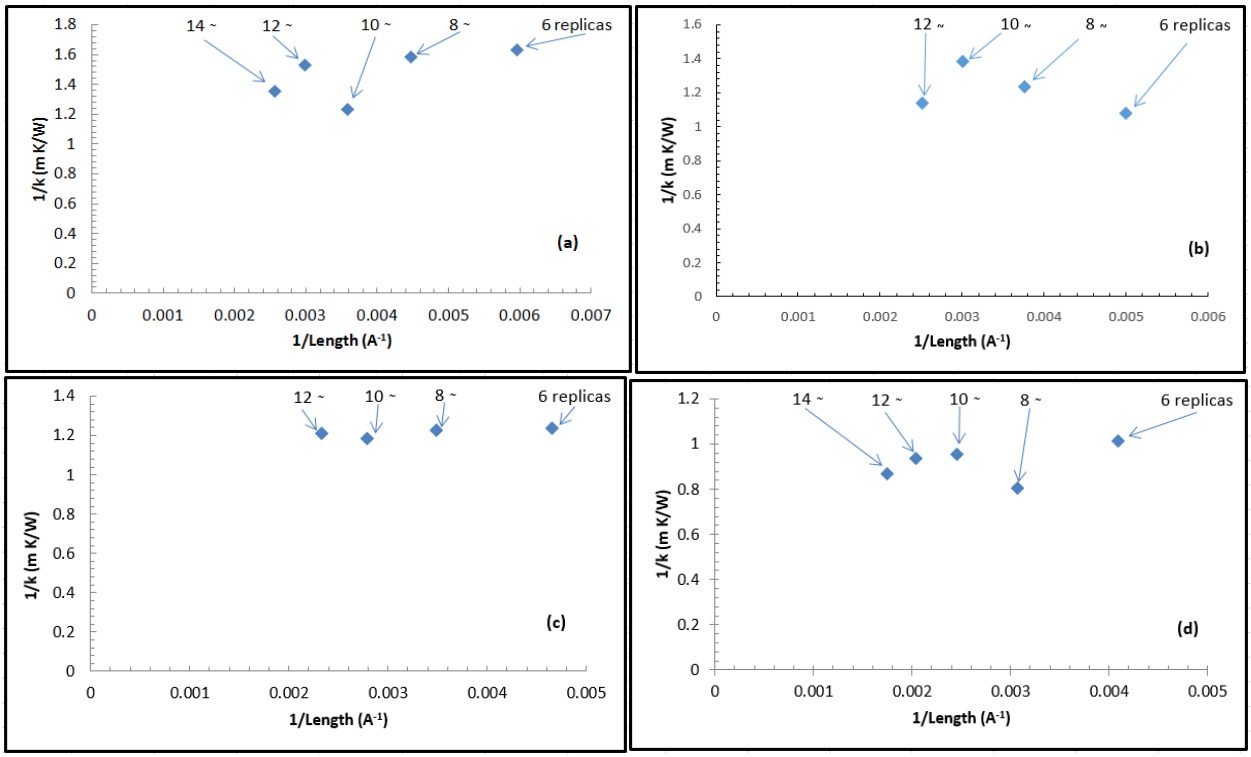

Figure 3-13: Inverse of the thermal conductivity in the x-direction versus inverse of the length of the stacked layers for different number of replicas for (a) $C_{20}H_{42}$, (b) $C_{24}H_{50}$, (c) $C_{26}H_{54}$ and (d) $C_{30}H_{62}$

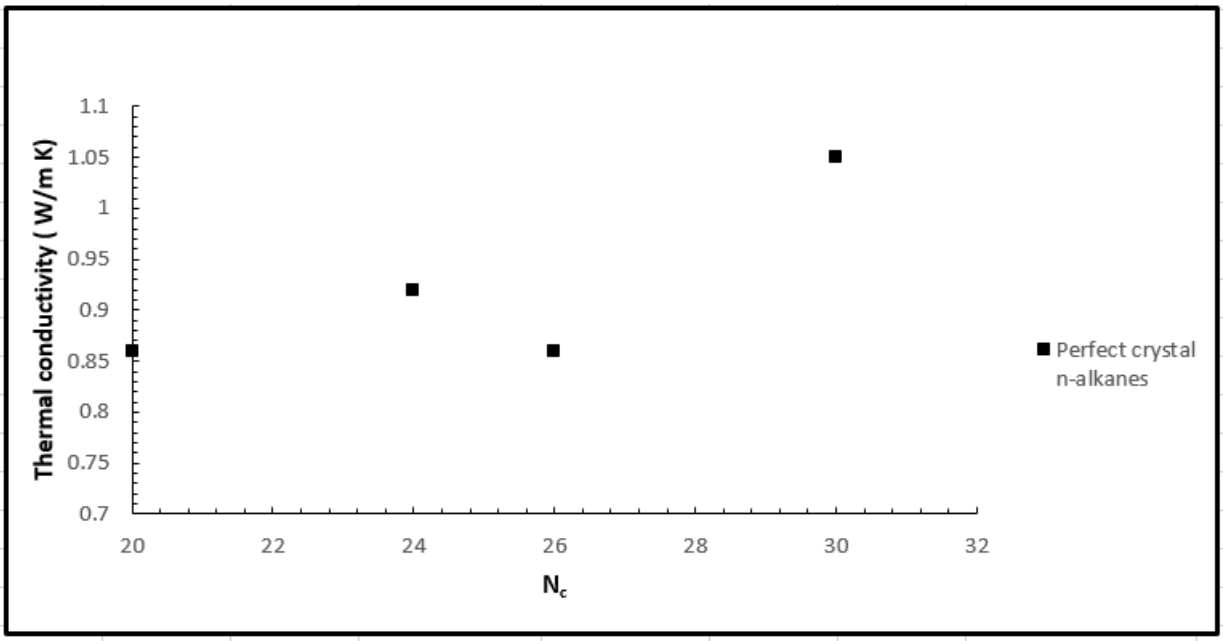

Figure 3-14: Thermal conductivity values for perfect crystal n-alkanes at T = 270 K versus the number of carbon atoms within the chain

Figure 3-15: N-Hexacosane ($C_{26}H_{54}$) solid samples obtained following the oven solidification process (approximately diameter of 2.5 cm and thickness of 1 cm) (sides shown in the figure were exposed to the atmosphere)

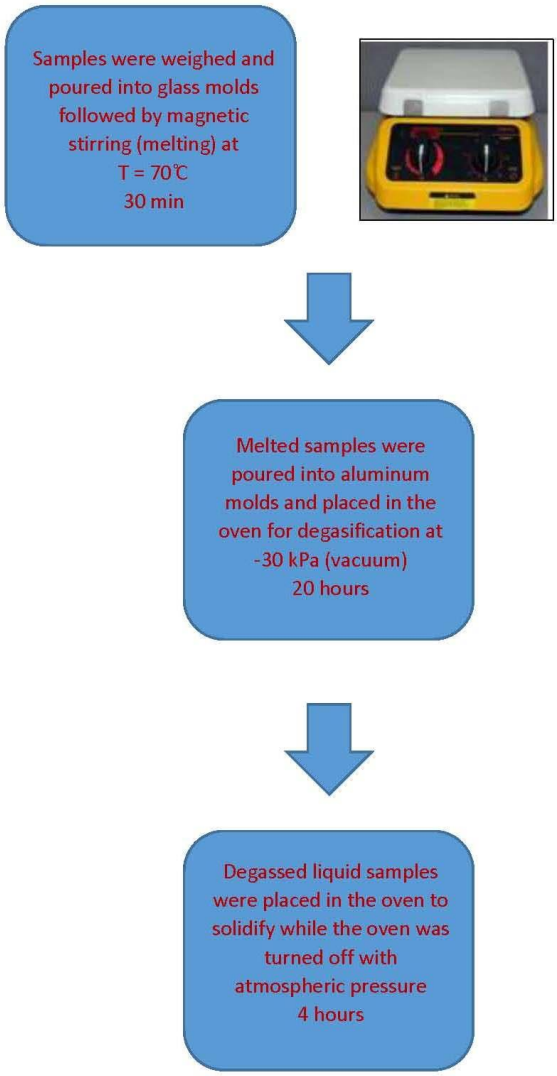

Figure 3-16: Schematic diagram for preparation of the solid samples

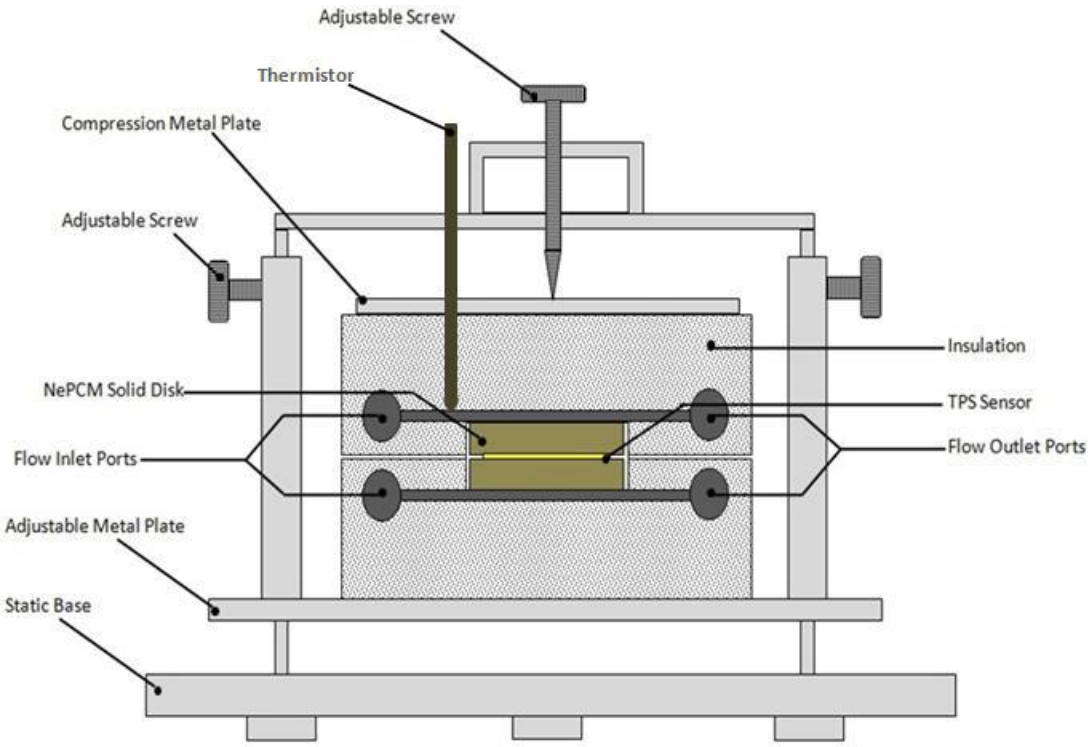

Figure 3-17: Schematic view of the support set-up for the samples supplied with the TPS 500 instrument (Hot Disk AB, Gothenburg, SWEDEN) (taken from M. Nabil, 2013)

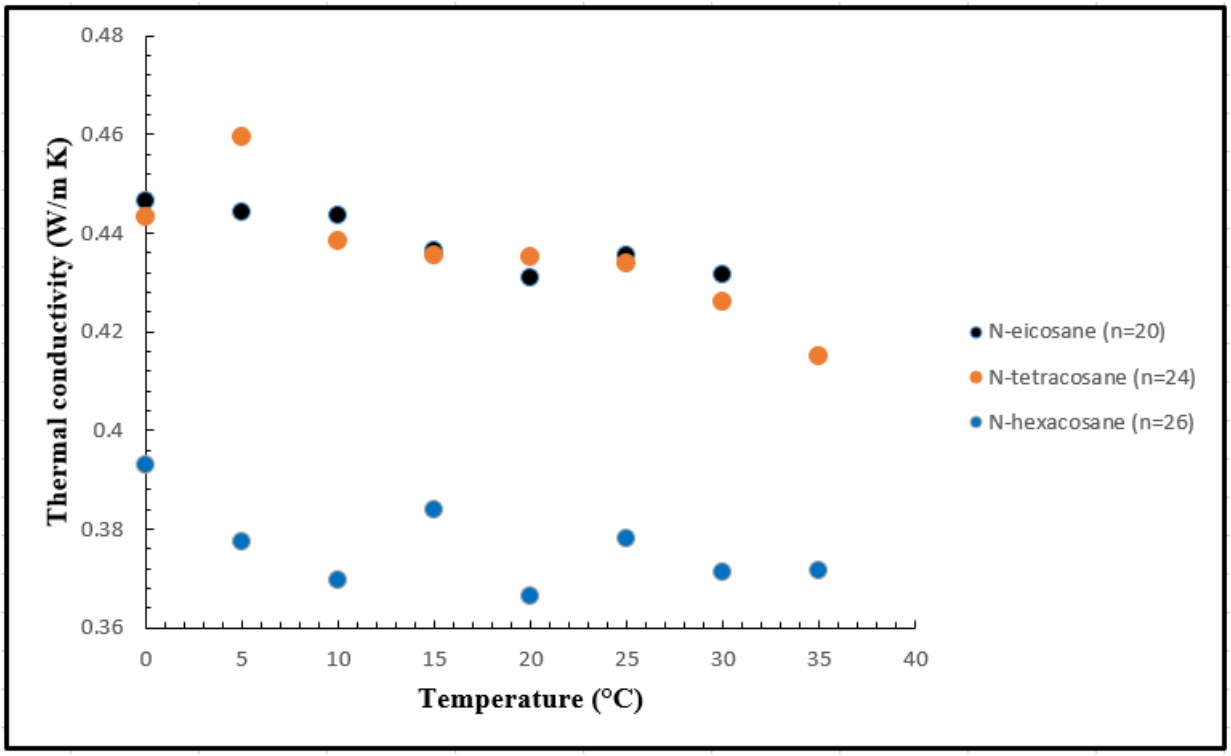

Figure 3-18: Experimental thermal conductivity values of the three n-alkanes (n=20, 24 and 26) as a function of temperature

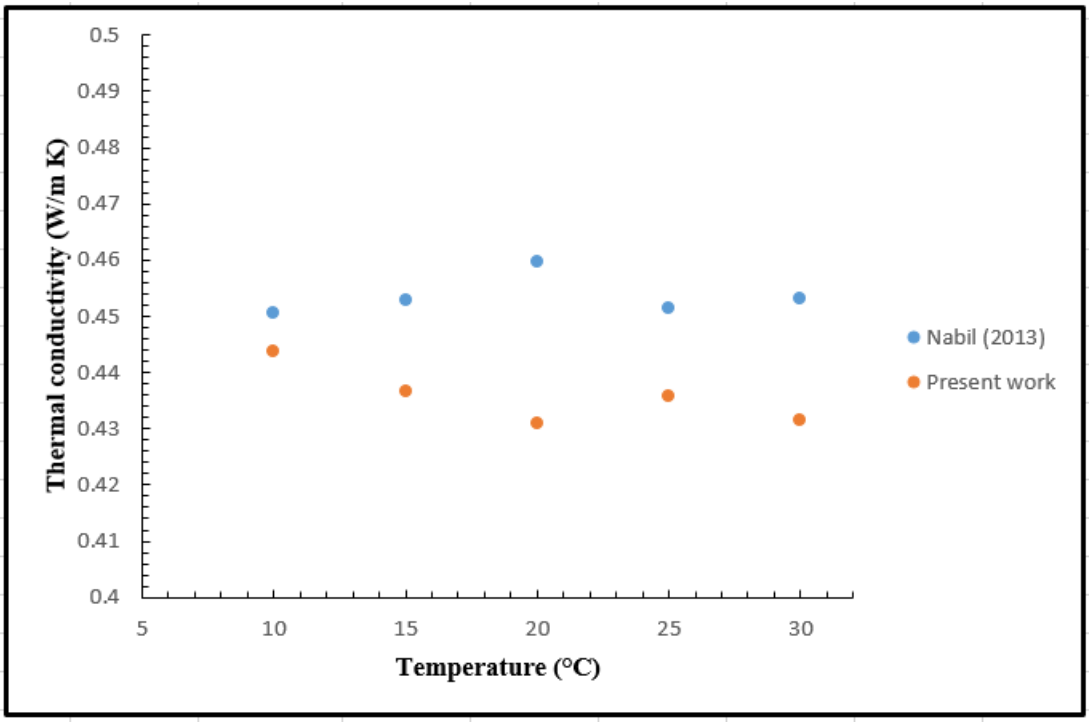

Figure 3-19: Comparison between experimental data of Nabil (2013) and the current experimentally-determined thermal conductivity values of n-eicosane at different temperatures

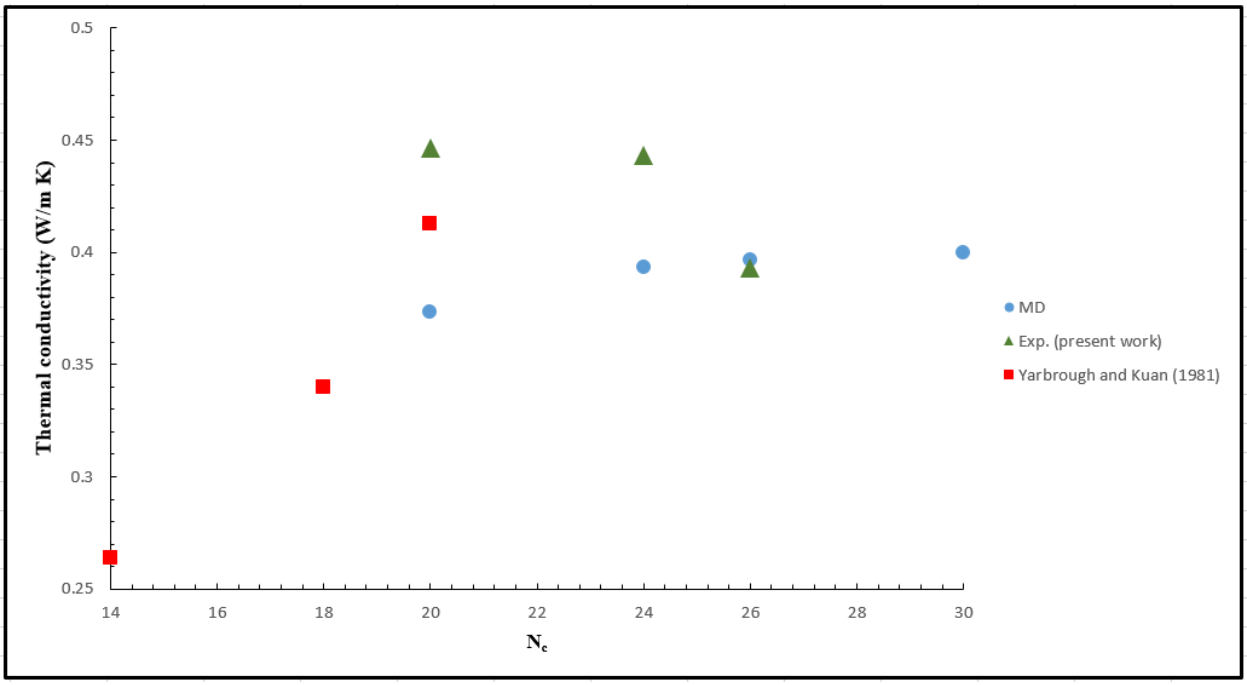

Figure 3-20: Comparison between MD and experimental thermal conductivity values of present work and those of Yarbrough and Kuan (1981) for n-alkanes in solid phase (n=20, 24 and 26) at T = 0 °C

4. Chapter 4: The Thermal Interfacial Conductance between the Layers of N-alkane Molecules

4.1 Introduction

There are two important factors that determine effectiveness of heat transfer. Thermal conductivity of bulk materials is one factor which was discussed in the previous chapter in detail. The other important concept in heat transfer is the effect of the boundaries and interfaces on the conductive mode of heat transfer. Different factors such as defects across the interfaces, phonon mismatch, and temperature of the interfaces can affect heat transfer and make a marked impact on heat transport. It is possible that two materials with very high thermal conductivities combine at a junction (interface) and exhibit a very low effective thermal conductivity (combination of the thermal conductivity of the materials and the thermal interfacial conductance). In the previous chapter, the effect of the length of the n-alkanes molecules on the thermal conductivity of bulk n-alkanes was studied. In this chapter, we will investigate the thermal boundary conductance between the layers of perfect crystal n-alkanes. Theoretically, there are two main models that are utilized to predict the interfacial thermal conductance in the nanoscale, namely the acoustic mismatch model (AMM) and the diffusive mismatch model (DMM). In recent years, MD simulations have received greater attention for predicting the thermal boundary conductance between the junctions. Both NEMD and EMD simulations can be utilized to study this effect.

Section 4.2 of this chapter is a review on what have been done on this topic. Next section is about the NEMD and EMD simulations that were used to determine the interfacial thermal conductance between the layers of n-alkanes. Lastly, we will compare the results from the NEMD and EMD simulations for determining the thermal boundary conductance.

4.2 Literature Review

Work on the nanoscale transport across the boundaries and the interfaces has been less developed compared to studies devoted to phonon transport in bulk materials. Thermal boundary conductance, which is the inverse of the Kapitza resistance (Kapitza, 1941) relates the temperature discontinuity at the interface to the associated heat flux. Attempts to predict the thermal interfacial conductance have led to development of two main models that are called the acoustic mismatch model (AMM) and the diffusive mismatch model (DMM). AMM is based on the classical wave theory and acoustics (Swartz and Pohl, 1989). Completely specular scattering is assumed in this model which means that all the incident phonons are assumed to be transmitted to the other side of the interface. AMM determines the transmissivity based on the phonon modes, wave number and the wave vectors (acoustic impedance). However, real interfaces are not perfect and exhibit some measure of roughness or the material might be at higher temperatures which AMM method is not suitable to use for these conditions. The DMM approach was introduced to address these deficiencies of the AMM technique. DMM calculates the transmission probability based on the group velocity and the density of states. Norris et al. (2013) reviewed the effect of different factors such as the interface mismatch, temperature, roughness and etc., as well as the effects due to multilayered structures on the thermal boundary conductance. For more detailed information, the reader is encouraged to refer to Swartz and Pohl (1989), Chen (2000), Cahill et al. (2002) and a recent review by Pop (2010).

MD simulations have exhibited great potential as an appropriate numerical solution to the thermal boundary conductance phenomenon within materials. Both EMD (Barrat and Chiaruttini, 2003) and NEMD (Barrat and Chiaruttini, 2003, Shenogin et al., 2004, and Hu et al., 2011) approaches have been carried out for MD determination of the thermal boundary conductance.

EMD uses a Green-Kubo-based formula to determine the conductance through evaluating the autocorrelation function of the power crossing the interface. In this method, the transport property is related to the corresponding microscopic fluctuations at equilibrium, whereas in NEMD, either a transient or a steady-state temperature change is imposed in the system.

Stevens et al. (2007) and Hu et al. (2011) utilized MD simulations to investigate the effect of the interface temperature on the thermal interfacial conductance and they found that thermal interfacial conductance increase with the temperature of the interface.

Merbia and Termentzidis (2012) compared the results of the NEMD and EMD simulations for determining the thermal boundary conductance of solid layers. They stated that the thermal boundary conductance values using the EMD simulations differ from those of the NEMD simulations where this difference reaches a factor of five for common semiconductors.

Liang et al. (2013) utilized both the EMD and NEMD simulations to study the thermal conductance at solid-gas interfaces with different interfacial bonding strengths. They stated that the EMD simulation results agree very well with the predictions based on the NEMD simulations.

4.3 Simulation methodology and model structures

4.3.1 NEMD simulations

4.3.1.1 Model structure

Perfect crystal structures of four different n-alkanes including $C_{20}H_{42}$, $C_{24}H_{50}$, $C_{26}H_{54}$ and $C_{30}H_{62}$ which were explained earlier in section 2.2.4.2 were utilized for this study as well. The same procedure was followed to determine the thermal boundary conductance (G_k) between the layers

of these structures. The base structure including 161 molecules was equilibrated under the *NPT* conditions at T = 150 K and atmospheric pressure for 5,000,000 time steps. The systems were then heated up to T = 270 K for another 5,000,000 time steps and was equilibrated at T = 270 K under the *NPT* conditions over 3,000,000 time steps. Similar to the case for the thermal conductivity of the perfect crystal structure of n-alkanes, in order to determine G_k of the perfect crystal structures, the base structures were replicated in the molecular axis direction for 6, 8, 10, 12 and 14 times. The system was then equilibrated under the NVT conditions for 3,000,000 time steps where the system attained steady state. The value of the heat flux was chosen to be 0.005 kcal/mol and imposed over the structure for 5,000,000 time steps. The resulting temperature profiles for a perfect crystal stacked structure (6 times) are shown in Figure 4-1. The temperature profiles were averaged over the last 1,000,000 time steps of heat flux addition. Also note that the size of the simulation boxes varied even though the number of molecules was fixed at 161.

4.3.1.2 Methodology

We utilized the NEMD simulations to determine G_k directly. As can be seen in Figure 4-1, the temperature profiles for the perfect crystal structures are nearly flat within each layer and there are temperature jumps at the interfaces between the neighboring layers. This temperature difference between the neighboring layers is related to the thermal resistance between the layers. G_k can be calculated directly from the formula:

$$G_k = \frac{q}{\Delta T}. \tag{4.1}$$

Average of all these temperature differences (ΔT) is calculated and upon dividing flux (q) by this average, one can determine the thermal interfacial conductance (G_k) between the layers.

4.3.1.3 Results

The thermal boundary conductance between the n-alkanes layers were determined using the NEMD method for different number of replications (Table 4-1) and the averaged values are given in Table 4-2. G_k values from the NEMD method are plotted as a function of the length of the n-alkane molecules in Figure 4-2. As can be seen in Figure 4-2, NEMD-based thermal interfacial conductance of the n-alkanes exhibit nearly no dependence on the number of carbon atoms within the n-alkanes molecule chains.

4.3.2 EMD simulations

4.3.2.1 Model structure and simulation methodology

Three n-alkanes (n=20, 26 and 30) were selected for this study. Three (3) layers of each molecule were aligned in a perfect crystal structure (Figure 4-3). The structure was then equilibrated under the same conditions as the NEMD method. $C_{24}H_{50}$ (n=24) was not included in this study at the outset. After the results were obtained for EMD-determined thermal boundary conductance, no more work was done on this part.

Equilibrium molecular dynamics (EMD) simulations was also carried out to determine G_k. In using this method, G_k will be calculated using the Green-Kubo formula:

$$G_k = \frac{1}{Ak_BT^2}\int_0^\infty < p(t)p(0) > dt, \tag{4.2}$$

where the symbol < > denotes the ensemble average, A is the cross sectional area of the solid surface, t is time, and p is the fluctuating heat power across the interface which can be computed by $p\ (t) = dE_{gas}\ (t)\ /dt$, where E_{gas} is the instantaneous internal energy of the layer of molecules.

The structure was equilibrated under the same conditions as the NEMD method. The total energy of the middle layer was recorded for calculating the power and the auto-correlation. The correlation time was chosen to be 32000 time steps (80 ps). Five (5) other simulations were performed for the same structure with different initial velocity distribution conditions to check on the repeatability of the simulations.

According to Liang et al. (2013), integration of the power auto-correlation function (PACF) contains information about the thermal boundary conductance. G_k can then be determined by fitting the tail of the integration of the power auto-correlation function (PACF) by the exponential functions.

4.3.2.2 Results

Time variation of the PACF and the integrated value of the PACF for $C_{20}H_{42}$ n-alkane are shown in Figures 4-4 and 4-5, respectively. The red part of the graph in Figure 4-5 is the tail of the graph that was used to determine the thermal boundary conductance values by fitting the tail with the exponential function as was discussed earlier in section 3.3.2.1. The thermal boundary conductance values from the EMD simulations are shown in Figure 4-6. It should be noted that the error bars for the values obtained from the EMD method are sizeable (with a standard deviation of nearly 10 MW/m^2 K for the cases studied).

4.4 Comparison between the NEMD and EMD results

Table 4-2 summarizes all the thermal boundary conductance values for the n-alkanes using the NEMD and EMD methods and these values are also shown in Figure 4-7. Both the NEMD and EMD simulations exhibit nearly no change in the value of G_k with the molecular length. However, the values obtained from the EMD simulations are consistently less than the values

from the NEMD simulations with this difference reaching a factor of nearly five (5) in most cases. Merbia and Termentzidis (2012) mentioned the same behavior for study of semi-conductors of their work.

4.5 Summary

In summary, the interfacial thermal conductance, G_k, between the layers of perfect crystal structure of n-alkanes molecules is studies utilizing both the NEMD and EMD methods. It is shown that the thermal boundary conductance has almost no dependence on the length of the molecules. G_k values obtained from the NEMD method were all in the same range and exhibited repeatability. However, the EMD-determined G_k values exhibit big error bars which is common in the EMD methodology. Six (6) simulations with different initial conditions were run to check on the repeatability of the simulations for the EMD method. The G_k values obtained from the EMD simulations are less than the values from the NEMD simulations where this difference reaches a factor of nearly five (5) in most cases.

Table 4-1: Thermal boundary conductance values for different number of replications for the n-alkanes using the NEMD method

N-alkanes / Replicas		n-eicosane $C_{20}H_{42}$	n-tetracosane $C_{24}H_{50}$	n-hexacosane $C_{26}H_{54}$	n-triacontane $C_{30}H_{62}$
G_k (NEMD) ($MW/m^2 K$)	6	172.4	221.9	183.4	161.6
	8	204.1	228.9	208.3	208.6
	10	254.2	207.3	221.6	215.5
	12	223.7	243.8	218.5	243.7

Table 4-2: Summary of the thermal boundary conductance values obtained from the NEMD and EMD methods

N-alkanes	n-eicosane $C_{20}H_{42}$	n-tetracosane $C_{24}H_{50}$	n-hexacosane $C_{26}H_{54}$	n-triacontane $C_{30}H_{62}$
G_k (NEMD) ($MW/m^2 K$)	214	219	216	212
G_k (EMD) ($MW/m^2 K$)	39	-	34	46

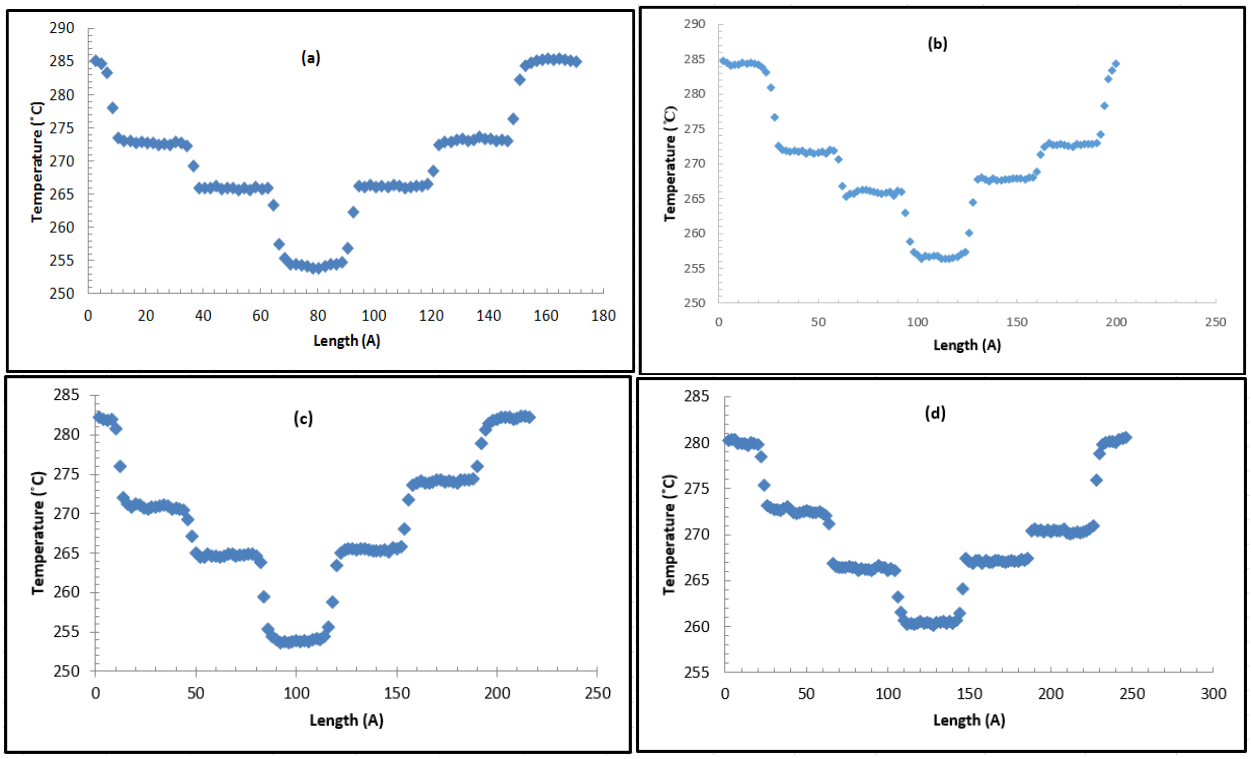

Figure 4-1: Temperature profiles for the case of perfect crystals with six (6) replications in response to the imposed heat flux for (a) $C_{20}H_{42}$, (b) $C_{24}H_{50}$, (c) $C_{26}H_{54}$ and (d) $C_{30}H_{62}$

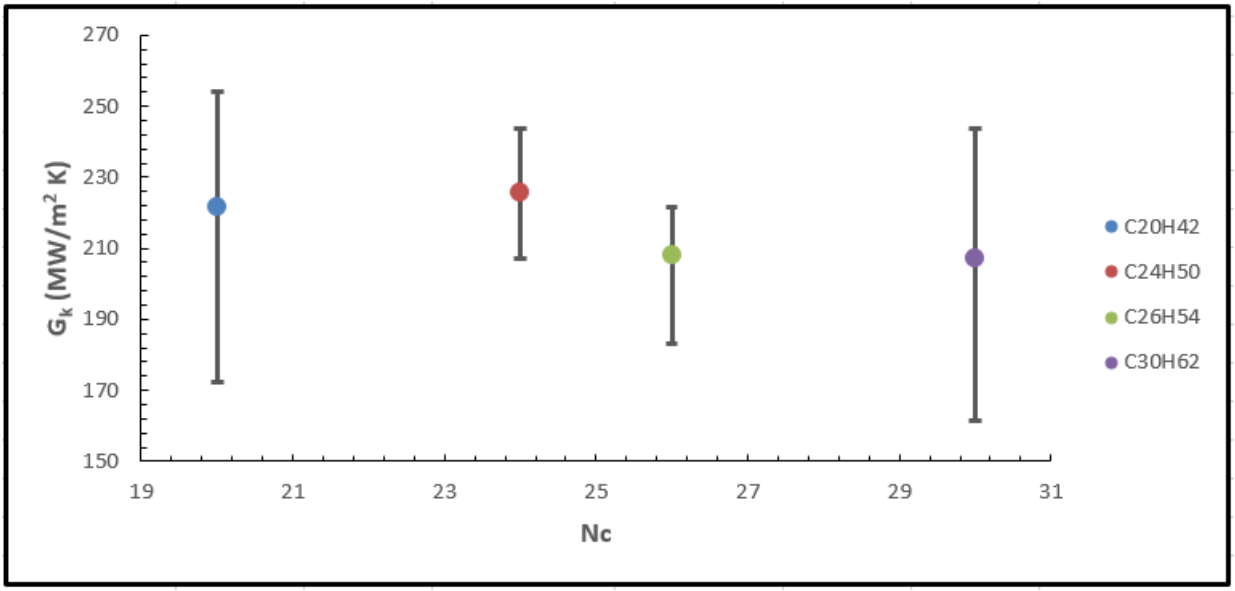

Figure 4-2: Thermal boundary conductance values for n-alkanes (n=20, 24, 26 and 30) utilizing the NEMD method

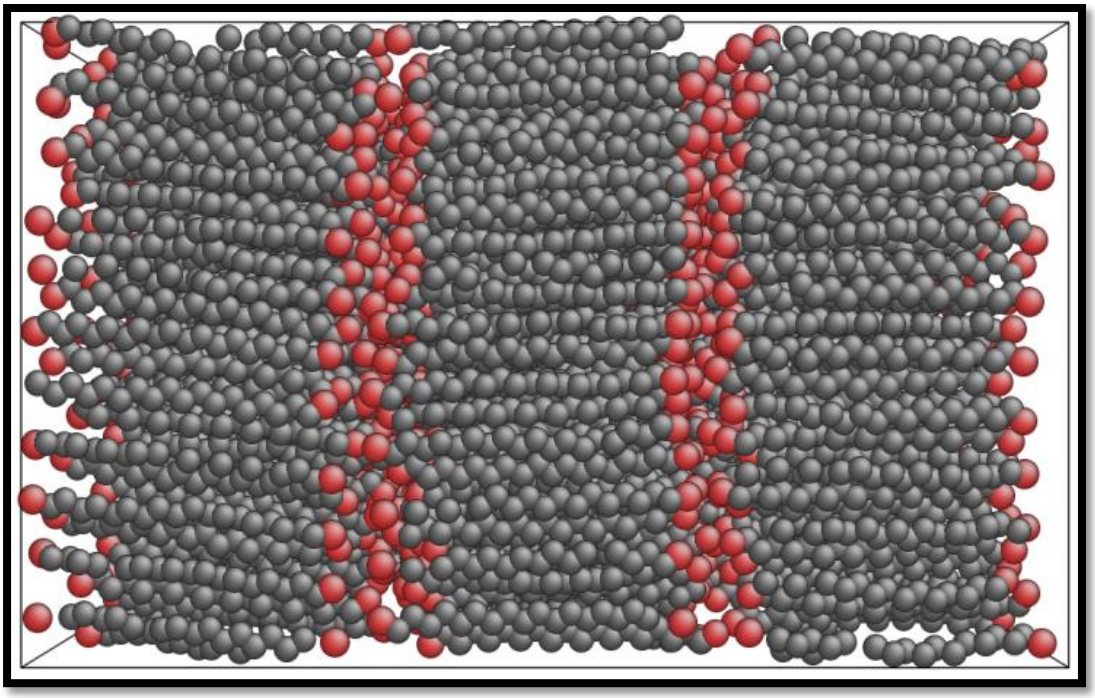

Figure 4-3: Snapshot of the system of three stacked n-eicosane (n=20) molecule layers after equilibration utilizing the EMD method (red balls shown as -CH_3 groups and grey balls as -CH_2- groups)

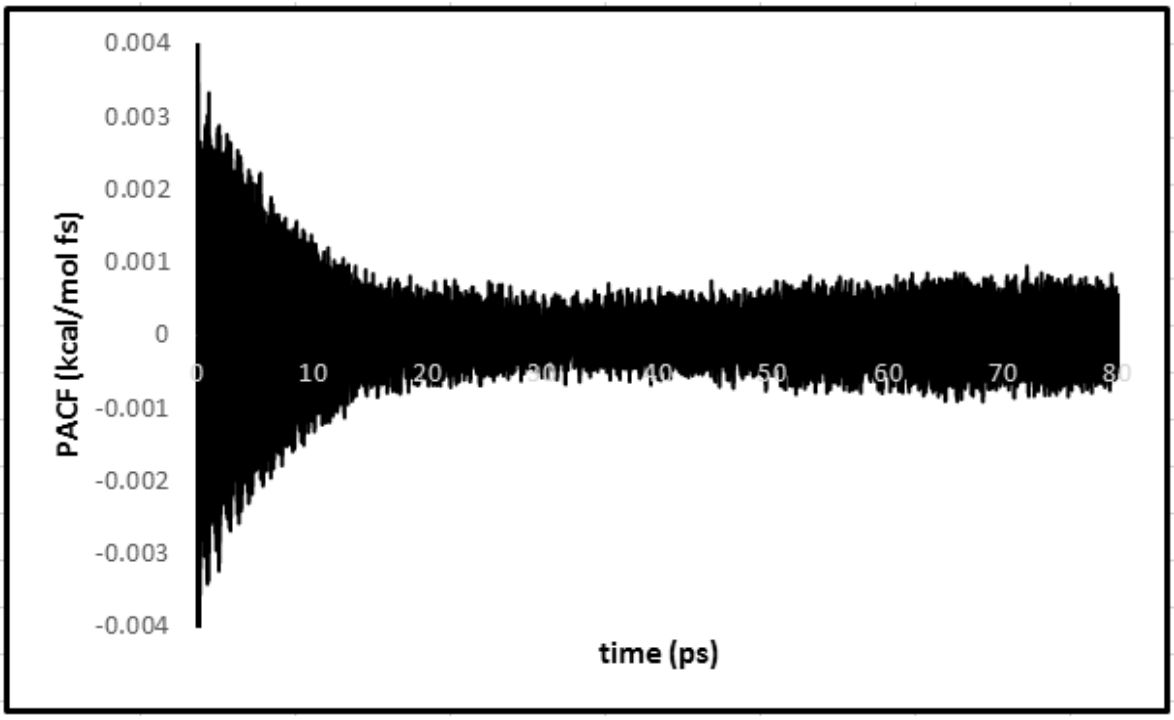

Figure 4-4: Power auto-correlation function (PACF) for $C_{20}H_{42}$ molecules as a function of time

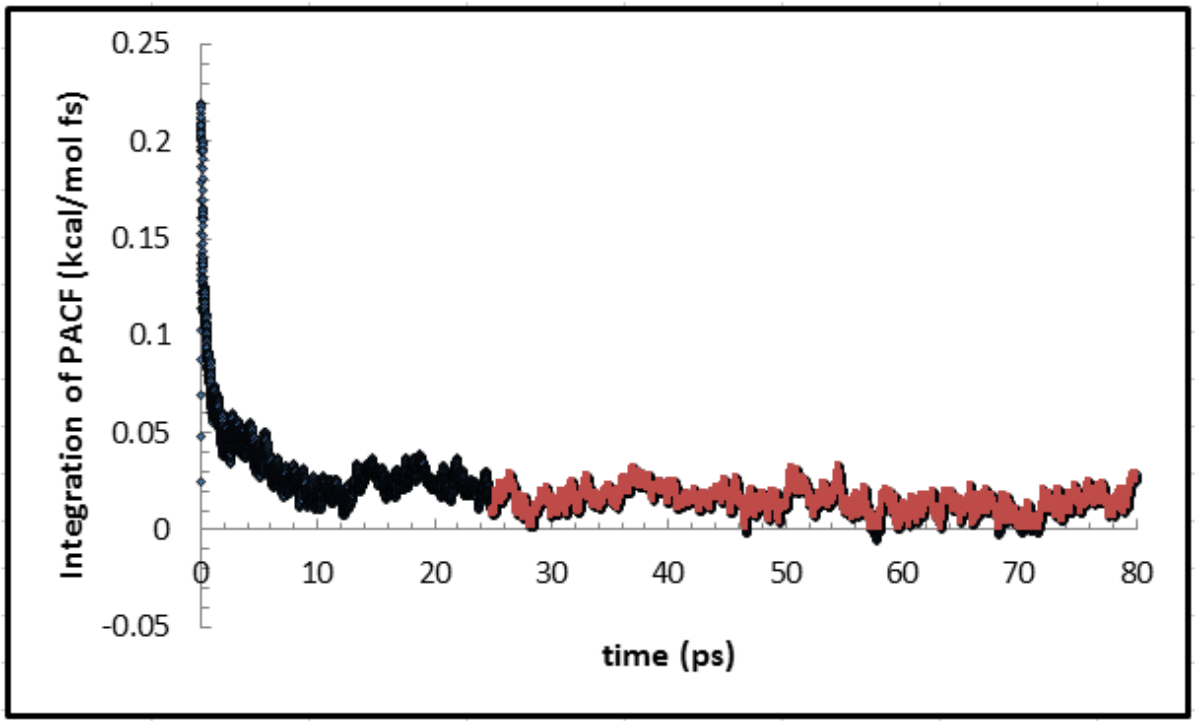

Figure 4-5: Integrated value of the PACF for $C_{20}H_{42}$ molecules as a function of time (red part is the tail of the graph)

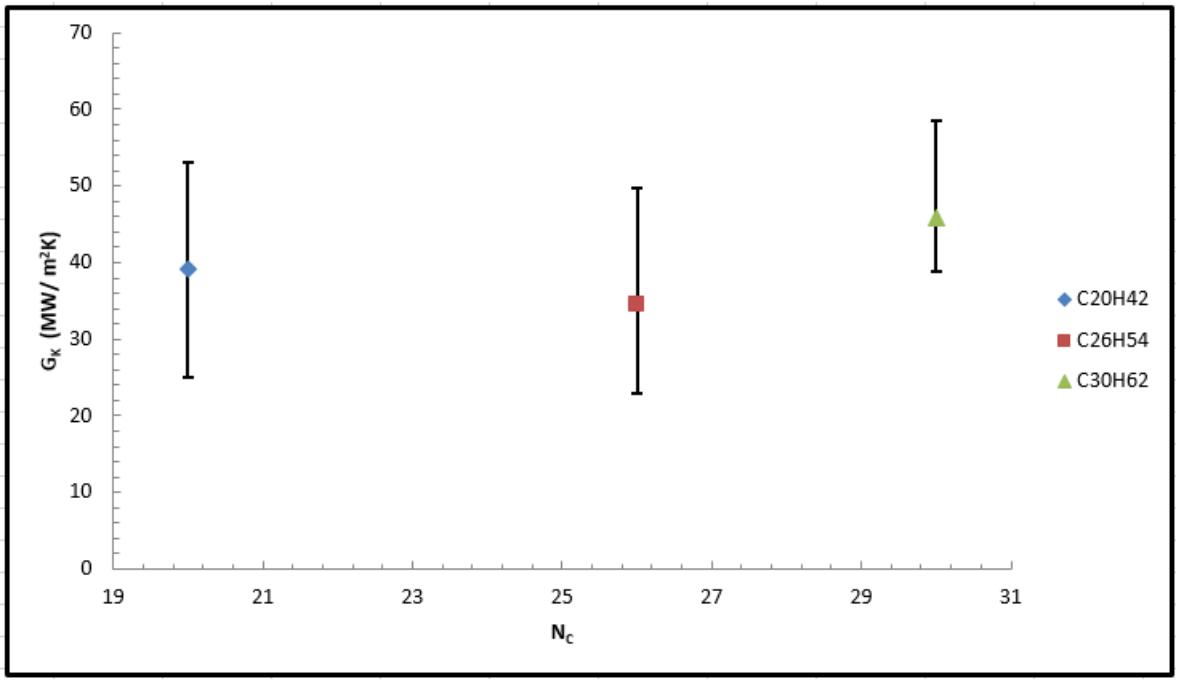

Figure 4-6: Thermal boundary conductance determined by the EMD method vs. the number of carbon atoms within the n-alkanes molecule chains

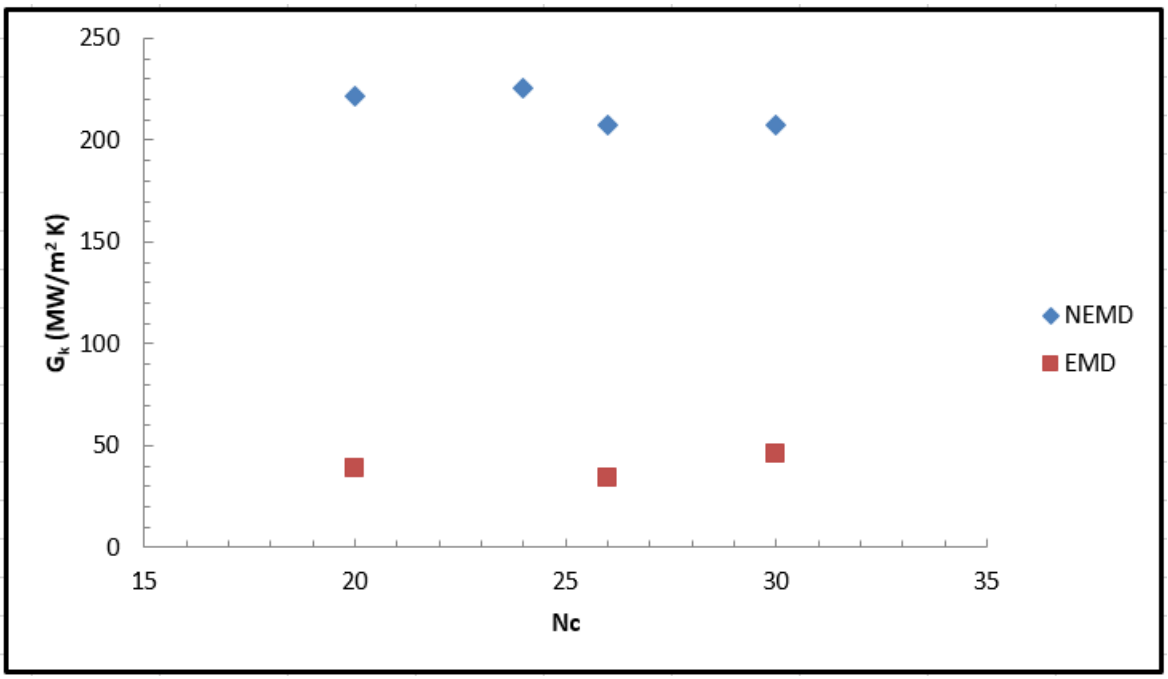

Figure 4-7: Comparison between the values of the thermal boundary conductance obtained from the NEMD and EMD methods

5. Chapter Five: Conclusions

In this chapter, conclusions pertinent to the molecular dynamics simulations and experimental determination of the thermal conductivity of long chain n-alkanes are presented.

Firstly in this thesis, the nanoscale thermal transport within long chain n-alkanes was investigated utilizing molecular dynamics simulations. Specifically, the effect of the length of n-alkane molecules on the thermal conductivity of n-alkanes and the thermal interfacial conductance between the layers of n-alkanes was studied. Thermal conductivity of some long chain n-alkanes was also measured experimentally using the TPS method and the results were compared with those of the MD simulations.

- **Thermal conductivity of n-alkanes:**

Molecular dynamics simulations were utilized to investigate the nanoscale thermal transport for both liquid and solid n-alkanes. The solid phase n-alkanes exhibit a more organized structure compared to the liquid systems, where crystalline nano-domain structures are clearly observed. Structural organization of the solid n-alkanes was quantified using the alignment factor when compared to the randomly-oriented molecules in the liquid systems. This suggests that as the structure becomes more organized, it will result in higher thermal conductivity values. Moreover, it is shown that the perfect crystal structures exhibit higher thermal conductivities compared to the solid structures. This can also be a proof to the fact that if the molecules in the system align in an organized structure, this will enhance the thermal conductivity.

Using molecular dynamics simulations, the thermal conductivity of four (4) n-alkanes (n = 20, 24, 26 and 30) in liquid, solid and perfect crystal phases was determined by the direct non-equilibrium molecular dynamics (NEMD) method. Imposing a heat flux over the samples will

lead to an associated temperature profile. Using the temperature gradient, heat flux value and the Fourier's relation, the thermal conductivity of these n-alkanes was calculated. Thermal conductivity values for liquid n-alkanes increase as the number of the carbon atoms within the chains increase which is consistent with the available experimental data in the literature. For the case of solid n-alkanes, there was no distinct relation between the thermal conductivity and the length of the n-alkane molecule. Thermal conductivity of $C_{24}H_{50}$ was higher than $C_{20}H_{42}$. As the number of the carbon atoms within the molecules increase from n=24 to n=26, thermal conductivity remained almost unchanged. Thermal conductivity of $C_{30}H_{62}$ was the highest among these solid n-alkanes. Overall, there is an increase in the thermal conductivity of solid n-alkanes as the length of the n-alkane molecules increases, however, we cannot conclude that thermal conductivity of solid n-alkanes rises with the number of the carbon atoms within the chains. The possible effect of anisotropy of the thermal conductivity tensor due to the structural organization of the solid phase was also investigated and was shown to be negligible. Perfect crystal n-alkanes follow a zigzag trend for thermal conductivity values with the number of the carbon atoms within the n-alkane molecules which is interesting because in previous studies of n-alkanes, this zigzag trend for other thermodynamic properties such as the melting point and etc. was reported.

The transient plane source (TPS) method was utilized to measure the thermal conductivity of three (3) pure n-alkanes (n = 20, 24 and 26) in the solid phase. The experimental thermal conductivity values of $C_{20}H_{42}$ agreed well with previous measured data of other researchers. It was shown that the thermal conductivities of $C_{20}H_{42}$ and $C_{24}H_{50}$ are very close to each other, whereas the thermal conductivity decreased for $C_{26}H_{54}$. This trend suggests that the thermal conductivity of n-alkanes goes down as the number of the carbon atoms within the n-alkane

molecules increase from n=20 to n=26 which is opposite of the results obtained from the MD simulations. However, we cannot conclude this suggested trend because the thermal conductivity of solid n-triacontane (n=30) is not measured experimentally.

- **Thermal boundary conductance:**

Thermal interfacial conductance between the layers of the perfect crystal n-alkanes was determined utilizing both equilibrium and non-equilibrium molecular dynamics (EMD and NEMD respectively) methods. The EMD method uses the Green-Kubo relation for the thermal boundary conductance which relates power fluctuations across the interfaces to the thermal boundary resistance. In the NEMD method, heat flux was directly imposed over the stacked perfect crystal n-alkane layers. Temperature drop/rise across each interface was related to the thermal boundary conductance between the neighboring layers. It is shown that the thermal interfacial conductance between the layers is not changing as the number of the carbon atoms within the n-alkane molecules increase. Both methods (NEMD and EMD) exhibit the same trend for the thermal interfacial conductance where no significant change in the thermal boundary conductance values was seen. However, values obtained from the EMD simulations are less than the values from NEMD simulations where this difference reaches a factor of nearly five (5) in most cases.

Bibliography

Babaei, Hasan, “Molecular-level modeling of thermal transport mechanisms within carbon nanotube/graphene-based nanostructure-enhanced phase change materials.” Diss. Auburn University, (2014), http://etd.auburn.edu/.

Babaei, Hasan, Keblinski P., and Khodadadi J. M., "Thermal conductivity enhancement of paraffins by increasing the alignment of molecules through adding CNT/graphene." International Journal of Heat and Mass Transfer, Vol. 58 Issue 1, pp. 209-216, (2013).

Barnes, J. D., "Inelastic neutron scattering study of the rotator phase transition in n-nonadecane." The Journal of Chemical Physics, Vol. 58, Issue 12, pp. 5193-5201, (1973).

Barrat, J.-L., and Chiaruttini, F., “Kapitza resistance at the liquid-solid interface.” Molecular Physics, 101(11), pp. 1605–1610, (2003).

Boese, Roland, Weiss H.-C., and Bläser D., "The Melting point alternation in the short-chain n-alkanes: single-crystal x-ray analyses of propane at 30 K and of n-butane to n-nonane at 90 K." Angewandte Chemie International Edition, Vol. 38, Issue 7, pp. 988-992, (1999).

Cahill, D. G., Ford, W. K., Goodson, K. E., Mahan, G. D., Majumdar, A., Maris, H. J., ... and Phillpot, S. R., “Nanoscale thermal transport.” Journal of Applied Physics, Vol. 93, Issue 2, pp. 793-818, (2003).

Chalmers, Bruce, "How water freezes." Scientific American, Vol. 200, pp. 114-122, (1959).

Chen, Gang, "Phonon heat conduction in nanostructures." International journal of thermal sciences, Vol. 39, issue 4, pp. 471-480, (2000).

Edberg, R., Evans, D. J., and Morriss, G. P., "Constrained molecular dynamics: Simulations of liquid alkanes with a new algorithm." The Journal of chemical physics, Vol. 84, Issue 12, pp. 6933-6939, (1986).

Esselink, K., Hilbers, P. A. J., and Van Beest, B. W. H., “Molecular dynamics study of nucleation and melting of n-alkanes.” The Journal of Chemical Physics, 101, 9033, (1994).

Fan, L. and Khodadadi, J. M., “Thermal conductivity enhancement of phase change materials for thermal energy storage: a review.” Renewable and Sustainable Energy Reviews, Vol. 15, pp. 24-46, (2011).

Fan, Liwu, “Enhanced thermal conductivity and expedited freezing of nanoparticle suspensions utilized as novel phase change materials.” Diss. Auburn University, (2011), http://hdl.handle.net/10415/2707.

Fang, Xin, et al., "Increased thermal conductivity of eicosane-based composite phase change materials in the presence of graphene nanoplatelets." Energy & Fuels, Vol. 27, issue 7, pp. 4041-4047, (2013).

Frenkel, Daan, "Simulations: The dark side." The European Physical Journal Plus, Vol. 128, Issue 1, pp. 1-21, (2013).

Hu, L., Desai, T. G., and Keblinski, P., “Determination of interfacial thermal resistance at the nanoscale.” Physical Review B, Vol. 83, Issue 19, 195423, (2011).

Jorgensen, W. L., Madura, J. D., Swenson, C. J., and Carol, J., “Optimized intermolecular potential functions for liquid hydrocarbons.” Journal of American Chemical Society, 106(22), pp. 6638-6646, (1984).

Kapitza, P. L., “The study of heat transfer in helium II.” Zh. Eksp. Teor. Fiz, Vol. 11, Issue 1, (1941) [English translation: Journal of Physics-USSR, 4, 181.]

Khodadadi, J. M., Fan Liwu, and Babaei H., "Thermal conductivity enhancement of nanostructure-based colloidal suspensions utilized as phase change materials for thermal energy storage: a review." Renewable and Sustainable Energy Reviews, Vol. 24, pp. 418-444, (2013).

Knight, Charles Alfred, "The freezing of supercooled liquids." 1-1, (1967).

Kubo, R., “Statistical-mechanical theory of irreversible processes. I. General theory and simple applications to magnetic and conduction problems.” Journal of the Physical Society of Japan, Vol. 12, Issue 6, pp. 570-586, (1957).

Landry, E. S., “Thermal transport by phonons across semiconductor interfaces, thin films and superlattices.” PhD thesis, Carnegie Mellon University, (2009).

Lennard-Jones, J. E., "On the Determination of molecular fields." Proc. R. Soc. Lond. A 106 (738), pp. 463–477, (1924).

Liang, Z., Evans, W. and Keblinski, P., “Equilibrium and nonequilibrium molecular dynamics simulations of thermal conductance at solid-gas interfaces.” Physical Review E, Vol. 87, Issue 2, pp. 022119, (2013).

Liang, Zhi, Evans, William, and Keblinski, P. "Equilibrium and nonequilibrium molecular dynamics simulations of thermal conductance at solid-gas interfaces." Physical Review E, Vol. 87, Issue 2, 022119, (2013).

Luo, T., and Lloyd J. R., "Equilibrium molecular dynamics study of lattice thermal conductivity/conductance of Au-SAM-Au junctions." Journal of Heat Transfer, Vol. 132, Issue 3, 032401, (2010).

Marbeuf, A., and Brown, R., “Molecular dynamics in n-alkanes: Premelting phenomena and rotator phases.” The Journal of Chemical Physics, 124, 054901 (2006).

Marechal, G., Ryckaert, J-P, and Bellemans, André, "The shear viscosity of n-butane by equilibrium and non-equilibrium molecular dynamics." Molecular Physics, Vol. 61, Issue 1, pp 33-49, (1987).

Martin, M. G., and Siepmann, J. I., “Transferable potentials for phase equilibria. 1. United-atom description of n-alkanes.” The Journal of Physical Chemistry B, Vol. 102, Issue 14, pp. 2569-2577, (1998).

Martínez, L., Andrade, R., Birgin, E. G. and Martínez, J. M., “Packmol: A package for building initial configurations for molecular dynamics simulations.” Journal of Computational Chemistry, Vol. 30, pp. 2157-2164, (2009).

Mehling, H. and Cabeza, L. F., “Heat and cold storage with PCM: An up to date introduction into basics and application.” Springer-Verlag, Berlin, GERMANY, (2008).

Merabia, Samy, and Termentzidis, K. "Thermal conductance at the interface between crystals using equilibrium and nonequilibrium molecular dynamics." Physical Review B, Vol. 86, Issue 9, 094303, (2012).

Murashov, Vladimir, and Mary Anne White, "Thermal conductivity of insulators and glasses." Thermal Conductivity. Springer US, pp. 93-104, (2004).

Nabil, Mahdi, and Khodadadi, J. M., "Experimental determination of temperature-dependent thermal conductivity of solid eicosane-based nanostructure-enhanced phase change materials." International Journal of Heat and Mass Transfer, Vol. 67, pp. 301-310, (2013).

Nabil, Mahdi. "Thermal Conductivity of Nanostructure-Enhanced Phase Change Materials: Measurements for Solid Eicosane-Based Copper Oxide and Carbon Nanotube Colloids and Numerical Modeling of Anomalous Measurements near Phase Transition." Thesis, Auburn University, (2013), http://hdl.handle.net/10415/3672.

Nath, S. K., Escobedo, F. A., and de Pablo, J. J., “On the simulation of vapor–liquid equilibria for alkanes.” The Journal of Chemical Physics, 108, 9905, (1998).

Norris, Pamela M., Le, Nam Q., and Baker, Christopher H., "Tuning phonon transport: from interfaces to nanostructures." Journal of Heat Transfer, Vol. 135, Issue 6, 061604, (2013).

Plimpton, S., “Fast parallel algorithms for short-range molecular dynamics.” Journal of Computational Physics, Vol. 117, pp. 1-19, (1995).

Pop, Eric, "Energy dissipation and transport in nanoscale devices." Nano Research, Vol. 3, Issue 3, pp. 147-169, (2010).

Rao, Z., Wang, S., and Peng, F., "Self diffusion and heat capacity of n-alkanes based phase change materials: A molecular dynamics study." International Journal of Heat and Mass Transfer, Vol. 64, pp. 581–589, (2013).

Rastorguev, Y. L., Bogatov, G. F. and Grigor'ev, B. A., "Thermal conductivity of higher n-alkanes." Chemistry and Technology of Fuels and Oils, Vol. 10, Issue 9, pp. 728-732, (1974).

Rigby, D. and Roe, R., "Molecular dynamics simulation of polymer liquid and glass. II. Short range order and orientation correlation." The Journal of Chemical Physics, Vol. 89, pp. 205280, (1988).

Ryckaert, J. P. and Klein, M. L., "Translational and rotational disorder in solid n-alkanes: constant temperature-constant pressure molecular dynamics calculations using infinitely long flexible chains." J. Chem. Phys. Vol. 85, Issue 3, (1986).

Schelling, P. K., Phillpot, S. R., and Keblinski, P., "Comparison of atomic-level simulation methods for computing thermal conductivity." Physical Review B, Vol. 65, Issue 14, pp. 1–12, (2002).

Sellan, D., Landry, E., Turney, J., McGaughey, A., and Amon, C., "Size effects in molecular dynamics thermal conductivity predictions." Physical Review B, Vol. 81, Issue 21, pp. 1–10, (2010).

Shenogin, S., Ozisik, R., "Xenoview: visualization for atomistic simulations." (2007).

Shenogin, S., Xue, L., Ozisik, R., Keblinski, P., and Cahill, D.G., "Role of thermal boundary resistance on the heat flow in carbon-nanotube composites." Journal of Applied Physics, Vol. 95, Issue 12, pp. 8136–8144, (2004).

Smit, B., Karaborni, S., and Siepmann, J. I., "Computer simulations of vapour-liquid phase equilibria of n-alkanes." Journal of Chemical Physics, 102, 2126, (1995).

Stevens, Robert J., Zhigilei Leonid V., and Norris Pamela M. "Effects of temperature and disorder on thermal boundary conductance at solid–solid interfaces: Nonequilibrium molecular dynamics simulations." International Journal of Heat and Mass Transfer, Vol. 50, Issue 19, pp. 3977-3989, (2007).

Stryker, P. C., and Sparrow, E. M., "Application of a spherical thermal conductivity cell to solid n-eicosane paraffin." International journal of heat and mass transfer, Vol. 33, issue 9, pp. 1781-1793, (1990).

Swartz, E. T., and Pohl, R. O., "Thermal boundary resistance." Reviews of Modern Physics, Vol. 61, Issue 3, pp. 605-668, (1989).

Ungar, G., and Masic, N., "Order in the rotator phase of n-alkanes." The Journal of Physical Chemistry, Vol. 89, Issue 6, pp. 1036-1042, (1985).

Vogelsang, R., Hoheisel, C., Paolini, G. V., and Ciccotti, G., "Soret coefficient of isotopic Lennard-Jones mixtures and the Ar-Kr system as determined by equilibrium molecular-dynamics calculations." Physical Review A, Vol. 36, Issue 8, pp. 3964-3974, (1987).

Wang, J., H. Xie and Z. Xin, "Thermal properties of paraffin based composites containing multi-walled carbon nanotubes." Thermochimica Acta, Vol. 488, pp. 39–42, (2009).

Wentzel, N., and Milner S. T., “Crystal and rotator phases of n-alkanes: A molecular dynamics study,” The Journal of Chemical Physics, 132, 044901 (2010)

Yarbrough, D. W. and Kuan, C. N., “The thermal Conductivity of Solid N-Eicosane, N-Octadecane, N-Heptadecane, N-Pentadecane and N-Tetradecane.” Proceedings of the 17th Int. Thermal Conductivity Conference, pp. 265-274, (1981).

Yaws, Carl L., “Handbook of Thermal Conductivity, Volume 3:: Organic Compounds C8 to C28.” Vol. 3, Gulf Professional Publishing, (1995).

Appendix A: Three Dimensional Fourier's Law and the Anisotropy Effect

The Fourier's Law can be written in vector and index notations as follows:

$$\bar{q} = -\bar{\bar{k}}\,\nabla T, \tag{A-1a}$$

$$q_i = -k_{ij}\frac{dT}{dX_j}, \tag{A-1b}$$

where $\bar{q}$ is the heat flux vector, $\bar{\bar{k}}$ is the thermal conductivity tensor and ∇T is the temperature gradient vector. Utilizing the three dimensional Cartesian coordinate system (X_1-, X_2- and X_3-coordinates), the Fourier's Law is re-written as the following equations:

$$q_1 = -k_{11}\frac{dT}{dX_1} - k_{12}\frac{dT}{dX_2} - k_{13}\frac{dT}{dX_3}, \tag{A-2}$$

$$q_2 = -k_{21}\frac{dT}{dX_1} - k_{22}\frac{dT}{dX_2} - k_{23}\frac{dT}{dX_3}, \tag{A-3}$$

$$q_3 = -k_{31}\frac{dT}{dX_1} - k_{32}\frac{dT}{dX_2} - k_{33}\frac{dT}{dX_3}, \tag{A-4}$$

where q_i (i =1, 2 and 3) is the heat flux component in the *i*-th direction, k_{ij} is thermal conductivity tensor and $\frac{dT}{dX_j}$ is the temperature gradient due to the heat flux. The thermal conductivity tensor can be shown as follows:

$$k_{ij} = \begin{bmatrix} k_{11} & k_{12} & k_{13} \\ k_{21} & k_{22} & k_{23} \\ k_{31} & k_{32} & k_{33} \end{bmatrix}. \tag{A-5}$$

As was discussed in chapter 3 (section 3.3.3.1), the solid n-alkane samples exhibit a crystalline structure with observable and quantified grain boundaries. The nano-crystalline domains in the solid structures may introduce the anisotropy effect in the case of thermal conductivity

determination. Thus, to address this effect, the temperature profiles in the y- and z-directions due to the imposed heat flux in the x-direction were also obtained. As was expected, there was no noticeable temperature change in the y- and z-directions. The temperature variations in the y- and z-directions are shown in Figures A-1 and A-2 for the solid $C_{20}H_{42}$ (shortest chain), respectively, whereas the temperature variations in the y- and z-directions are shown in Figures A-3 and A-4 for $C_{30}H_{62}$ (longest chain), respectively. It is observed that the temperature variations in the y- and z-directions (due to the heat flux through the x-direction) fluctuate about an average temperature value. The values of the maximum temperature difference in all three spatial directions due to the heat flux in the x-direction are given in Table A-1. It can be inferred from the values in Table A-1 that there is no noticeable anisotropy for the base solid structure and the number of molecules were chosen such that this effect is negligible. In effect, the off-diagonal components of the thermal conductivity tensor ($k_{ij}, i \neq j$) are shown to be negligible. The determination of the dominant diagonal elements of the same matrix ($k_{ij}, i = j$) is presented in this thesis.

Table A-1: Maximum temperature difference in three directions (x-, y- and z-directions) due to heat flux in the x-direction for two n-alkanes

N-alkane		$C_{20}H_{42}$	$C_{30}H_{62}$
Maximum Temperature Difference, ºC	**X-Direction**	98.8	67.4
	Y-Direction	3.2	1.2
	Z-Direction	2.5	1.0

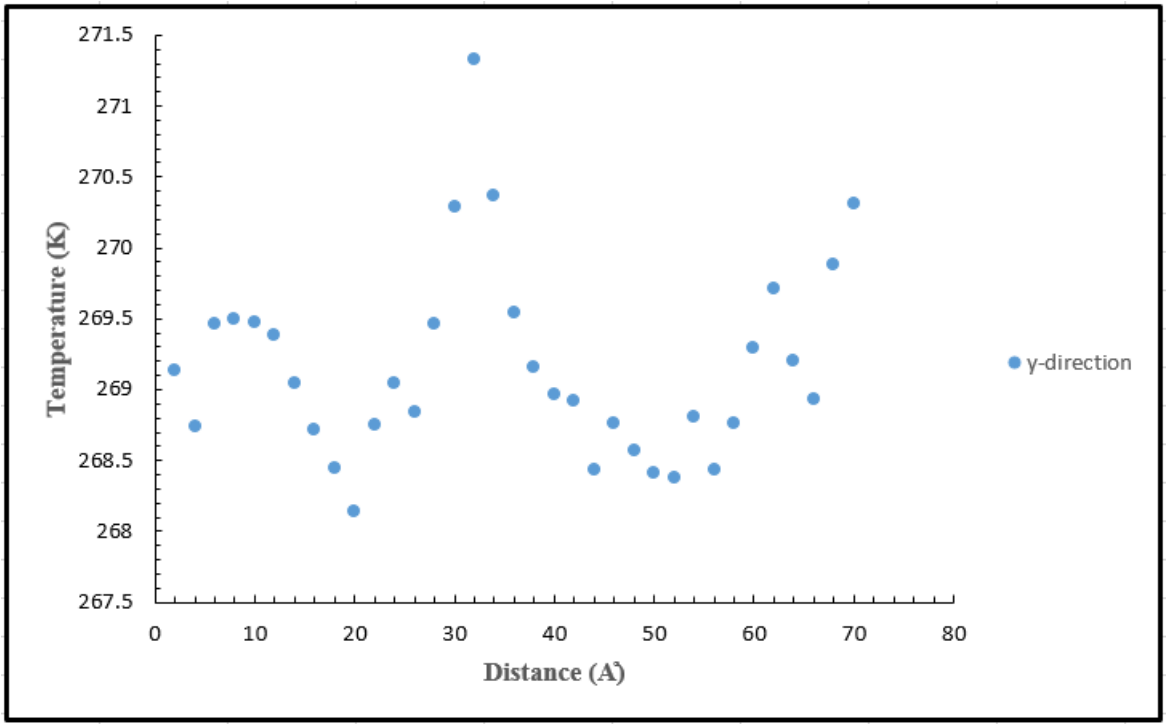

Figure A-1: Temperature profile in the y-direction due to the heat flux in the x-direction for solid n-$C_{20}H_{42}$

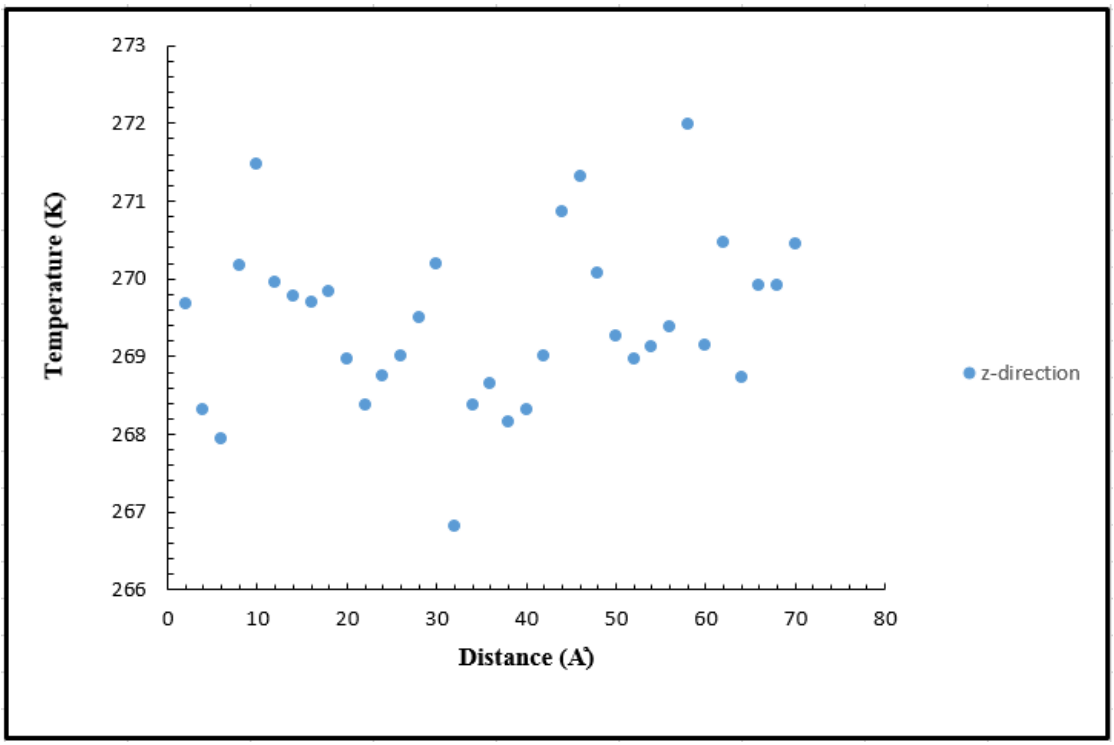

Figure A-2: Temperature profile in the z-direction due to the heat flux in the x-direction for solid n-$C_{20}H_{42}$

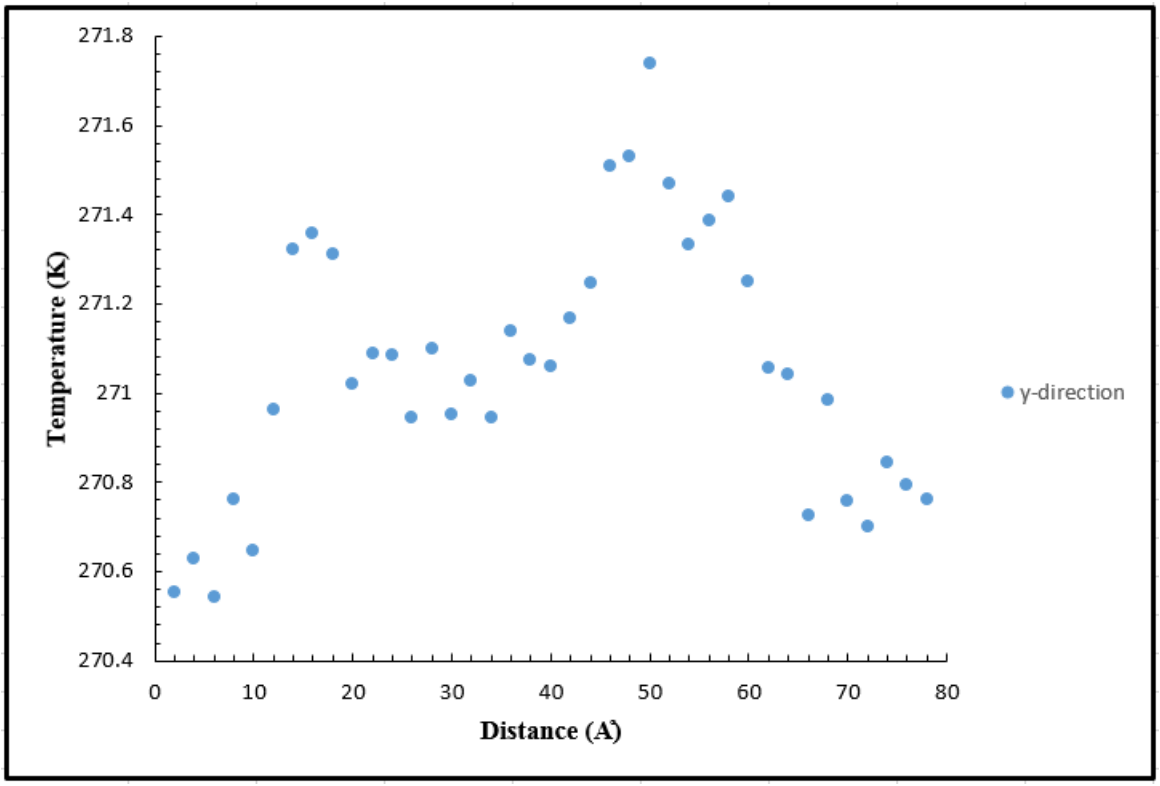

Figure A-3: Temperature profile in the y-direction due to the heat flux in the x-direction for solid n-$C_{30}H_{62}$

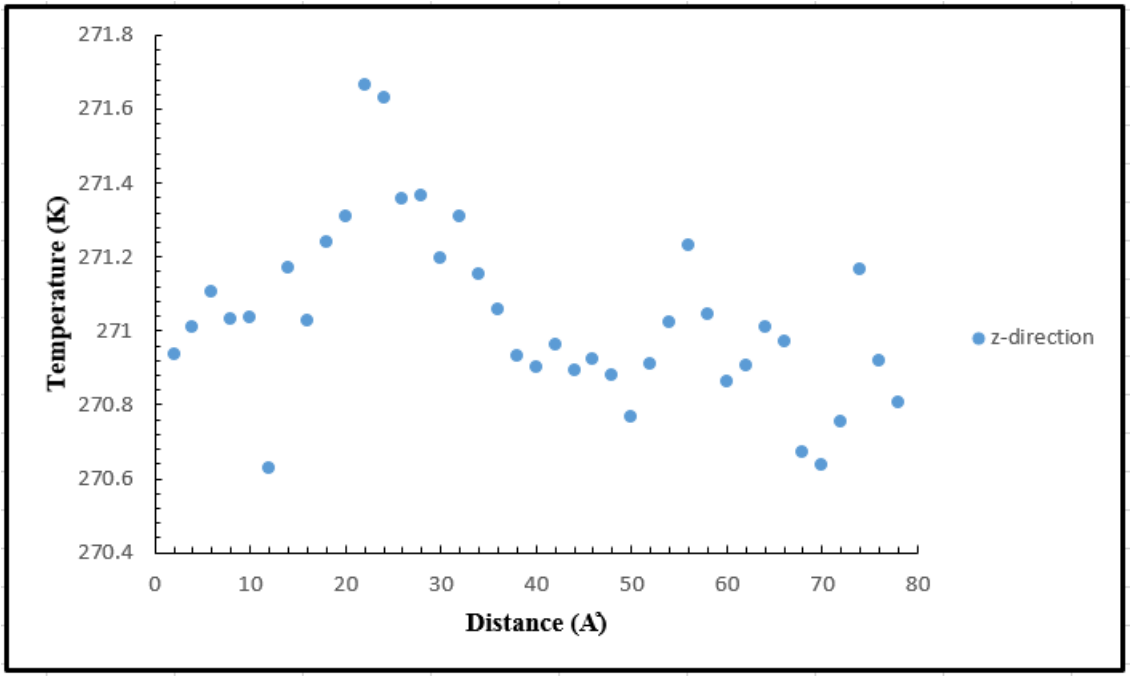

Figure A-4: Temperature profile in the z-direction due to the heat flux in the x-direction for solid n-$C_{30}H_{62}$